ASSESSMENT OF STEEL CABLE-STAYED PEDESTRIAN BRIDGE: ANALYTICAL MODELING AND ON-SITE VALIDATION

DEHA PEKER

ÖZYEĞİN UNIVERSITY

JULY, 2025

ASSESSMENT OF STEEL CABLE-STAYED PEDESTRIAN BRIDGE: ANALYTICAL MODELING AND ON-SITE VALIDATION

by
Deha Peker

Thesis
Submitted in Partial Fulfillment of the
Requirements for the Degree of

Master of Science

in
Civil Engineering

Advisor: Prof. Gülay Altay
Co-Advisor: Prof. Fuat Aras

Graduate School of Science and Engineering
Özyeğin University
İstanbul

July, 2025

ASSESSMENT OF STEEL CABLE-STAYED PEDESTRIAN BRIDGE: ANALYTICAL MODELING AND ON-SITE VALIDATION

Approved by:

Prof. Gülay Altay, Advisor
Department of Civil Engineering
Özyeğin University

Asst. Prof. Yiğit Can Altan
Department of Civil Engineering
Özyeğin University

Prof. Fuat Aras, Co-advisor
Department of Civil Engineering
İstanbul Medeniyet University

Asst. Prof. Derya Deniz
Department of Civil Engineering
Özyeğin University

Prof. Serdar Soyöz
Department of Civil Engineering
Boğaziçi University

Approval Date: July 2, 2025

To my family, Derya & Hakan PEKER

DECLARATION OF ORIGINALITY

I hereby declare that I am the sole author of this thesis and that this is the true copy of my thesis, including the final revisions, approved by my thesis committee. All data and information have been obtained, produced, and presented in accordance with the rules of research ethics and principles of academic honesty. As required by these rules, to the best of my knowledge, I have acknowledged ideas, thoughts, and any copyrighted material in accordance with the standard referencing rules. I certify that any part of this thesis has not been submitted for a degree or diploma in another educational institution.

Deha Peker

ABSTRACT

In this thesis study, the dynamic behaviour of a cable-stayed pedestrian bridge located in Istanbul is comprehensively investigated through both analytical modelling and experimental measurements. Based on the field observations, the geometry of the bridge, the dimensions of the structural elements, and the cross-section properties were identified, and a finite element model was created. To assess the dynamic characteristics, the natural frequencies and mode shapes were obtained by modal analysis, while the time-dependent responses of the structure were investigated by time history analysis, using real earthquake ground motion accelerations. In the experimental studies, ambient acceleration data were collected in three axes using accelerometers placed at specific points on the bridge deck. Operational modal analysis (OMA) techniques were employed, and dominant frequency components were extracted using Fast Fourier Transform (FFT). The comparison between the analytical and experimental results necessitated a model update process; within this scope, the two main parameters of the analytical model, mass and stiffness, were readjusted. The natural frequency results of the updated model's fundamental modes were observed to be closer to experimental data. This study delivers a calibrated and validated finite element model of the structure, and this model is intended to contribute to future studies involving the seismic analysis, vibration assessment, and structural health monitoring of similar bridge structures.

Keywords: Cable-stayed pedestrian bridge, Finite element modelling, Operational modal analysis, Model updating

ÖZET

Bu tez çalışmasında, İstanbul'da bulunan bir kablo askılı yaya köprüsünün dinamik davranışı, analitik modelleme ve deneysel ölçümler yoluyla kapsamlı bir şekilde incelenmiştir. Saha gözlemlerine dayanarak, köprünün geometrisi, yapısal elemanların boyutları ve kesit özellikleri belirlenmiş ve bir sonlu elemanlar modeli oluşturulmuştur. Dinamik özellikleri değerlendirmek için modal analiz ile doğal frekanslar ve mod şekilleri elde edilirken, yapının zamana bağlı tepkileri, gerçek deprem yer hareketi ivmeleri kullanılarak zaman tanım alanı analizi ile incelenmiştir. Deneysel çalışmalarda, köprü tabliyesinin belirli noktalarında yerleştirilen ivmeölçerler ile üç eksende ortam ivme verileri toplanmıştır. Operasyonel modal analiz (OMA) teknikleri kullanılmış ve Hızlı Fourier Dönüşümü (FFT) ile baskın frekans bileşenleri çıkarılmıştır. Analitik ve deneysel sonuçların karşılaştırılması, modelin güncellenmesini gerektirmiştir; bu kapsamda, analitik modelin iki ana parametresi olan kütle ve rijitlik yeniden ayarlanmıştır. Güncellenen modelin temel modlarının doğal frekans sonuçlarının deneysel verilere daha yakın olduğu gözlemlenmiştir. Bu çalışma, yapının kalibre edilmiş ve doğrulanmış bir sonlu elemanlar modelini sunmaktadır ve bu model, benzer köprü yapılarının sismik analizi, titreşim değerlendirmesi ve yapısal sağlık izlemesi ile ilgili gelecekteki çalışmalara katkıda bulunmayı amaçlamaktadır.

Anahtar Kelimeler: Kablo askılı yaya köprüsü, Sonlu elemanlar modeli, Operasyonel modal analiz, Model güncelleme

ACKNOWLEDGEMENTS

I would like to express my sincere gratitude to my advisor, Prof. Gülay Altay, who provided me with knowledge, experience, and support from the first day of my master's program until the last. Her guidance and academic contributions have been instrumental in every stage of my work.

I would also like to thank my co-advisor, Prof. Fuat Aras, for his technical support, endless assistance in fieldwork, and contributions.

I would like to express my gratitude to my friends who stood by me and supported me during my thesis work. Their moral support and motivation made this process easier and more productive for me.

Lastly, I would like to thank all the faculty members who guided me with their knowledge throughout my undergraduate and graduate education and contributed to the development of my academic perspective.

TABLE OF CONTENTS

LIST OF TABLES

LIST OF FIGURES

LIST OF SYMBOLS

A : Area

a : Acceleration

b : Width

c : Damping coefficient

C_e : Coefficient of elevation

C_f : Coefficient of friction

D : Diameter

DL : Dead Load

E : Elastic Section Modulus

EQ : Earthquake Load

f : Frequency (Hz)

f_n : Natural frequency (Hz)

F : Force

F_u : Ultimate Stress

F_y : Yield Stress

G : Shear Modulus

h : Depth

I_x : Moment of inertia about the x-axis

I_y : Moment of inertia about the y-axis

k : Stiffness

L : Length

LL : Live Load

M : Moment

M_3 : Moment about local 3-3 axis (SAP2000 terminology)

$[M]$: Mass Matrix

m : Weight

$m(t)$: Transmitted signal

R : Response modification factor

a_g : Earthquake acceleration (m/s^2)

r : Root radius

r_i : Inner rounding radius

r_o : Outer rounding radius

s : Sine

σ : Stress (Pa)

T : Period (s)

T_n : Natural period (s)

T : Transformation matrix

$u(t)$: Displacement as a function of time

$\dot{u}(t)$: First derivative of displacement with respect to time (velocity)

$\ddot{u}(t)$: Second derivative of displacement with respect to time (acceleration)

v : Velocity

$v(x)$: Transverse displacement as a function of x

V : Shear Force (N)

WL : Wind Load

ξ : Damping ratio

λ : Eigenvalue

ϕ : Mode shape (Eigenvector)

θ : Rotational freedom

ρ : Air Density

LIST OF ACRONYMS AND ABBREVIATIONS

AASHTO	American Association of State Highway and Transportation Officials
AISC	American Institute of Steel Construction
ANN	Artificial Neural Network
ASD	Allowable Stress Design
CFD	Computational Fluid Dynamics
EN	EuroNorm (European Standard)
PP	Peak Picking
FDD	Frequency Domain Decomposition
FEA	Finite Element Analysis
FEM	Finite Element Method
FFT	Fast Fourier Transform
SSI-COV	Covariance-Driven Stochastic Subspace Identification
SSI-DATA	Data-Driven Stochastic Subspace Identification
GFRP	Glass Fiber Reinforced Polymer
GPS	Global Positioning System
TMD	Tuned Mass Damper
PSD	Power Spectral Density
LTB	Lateral-Torsional Buckling
LRFD	Load and Resistance Factor Design
FEA	Finite Element Analysis

TS EN	Turkish Standard – European Norm
SNI	Standar Nasional Indonesia
SDOF	Single Degree of Freedom
MDOF	Multiple Degree of Freedom
PEER	Pacific Earthquake Engineering Research
OMA	Operational Modal Analysis
GPS	Global Positioning System

1. INTRODUCTION

Understanding the static and dynamic evaluation of cable-stayed bridges is increasingly drawing the attention of structural engineering, especially due to the increasing demand for lightweight and architecturally appealing bridge design. This work examines the static and dynamic behaviour of a steel cable-stayed pedestrian bridge in Taşdelen/Çekmeköy using analytical modelling and experimental validation methods.

The study's goal is to get accurate models of the bridge in question by calibrating the analytical model with data collected in the field and making sure that its behaviour closely matches that of the real structure. The validated model accurately reflects the behaviour of the existing structure and, by increasing the reliability of the model, thereby makes it possible to obtain results close to real outcomes in future analyses. Not only does it have a reliable model, but it also provides a solid basis for future design and enables early damage detection through long-term structural monitoring.

Studies on the design principles for bridges and characteristics of cable-stayed pedestrian bridges, along with various analysis methods and serviceability, are broadly covered in the literature. These studies emphasise the importance of proper and detailed modelling as well as verification of the accuracy of the values obtained from finite element analysis. Moreover, these studies underscore the significance of operational modal analysis in comprehending the dynamic behaviour of a bridge. The literature survey provides an important basis for the methodology and scope of the studies.

In this study, the cross-sectional properties of the bridge and the dimensions of the structural elements are determined by field inspections. The structural system of bridges ensures the stability, strength, and serviceability of the bridge. The superstructure consists of a main girder, which is built up from longitudinal and transverse beams with bracing elements for cross-sectional stability. The loads applied to the deck are transferred to pylons by cables in several ways to give the structure a pleasing appearance. In this bridge, the cables are used in parallel form and symmetrically to create a harp model. Pylons transfer the forces from the cables to foundations.

The structural design of the bridge includes the evaluation of dynamic effects such as dead loads, live loads, wind loads, and seismic loads to ensure overall safety and serviceability. The loads applied to the structure must comply with current standards and specifications. Load combinations for bridges differ from those for vertical structures, and the performance of a bridge is analysed under these specific load combinations. Section capacity checks are performed using a static design approach. Within the scope of static design, dead loads, live loads, and static wind loads are applied to the structure using finite element software, and the axial loads, shear forces, and moments acting on the elements are determined.

Determination of the dynamic properties of the bridge is a key and essential part of the study to ensure that the analytical frequencies of the Finite Element Method (FEM) closely match the measurement frequencies, confirming the accurate representation of the actual structure. If the frequency values are found not to be similar, the finite element model should be calibrated, and the causes for these differences should be re-evaluated. In the study, verification is made on natural frequencies and mode shapes, and the two important parameters are mass and stiffness. Further, in the modelling stage, in addition to the main elements, concrete slabs, railings, and stairs are also included in the mass of the system, and care is taken to ensure that the mass of the real structure and the mass of the model are sufficiently close to each other. The natural frequencies and mode shapes of the model are obtained by modal analysis, which is an important and easy analysis in determining the dynamic character of the structure in the basic way.

To validate the analytical results of the finite element model, measurements were conducted on-site at the bridge. Triaxial low-noise accelerometers are used to find experimental frequencies. In the first step, displacement data is acquired from measurements taken at the middle span. The Fast Fourier Transform (FFT) is employed to transform the displacement-time data into the frequency domain. The peak points where the amplitude reaches its maximum are identified, and experimental frequencies are obtained using the Peak Picking (PP) method. The experimental frequencies obtained from measurements are compared with the analytical frequencies found in FEM. Especially in bridges with high pedestrian traffic, comfort is an important criterion in terms of serviceability, and the acceleration-frequency values obtained in the measurements are evaluated for limit states in different codes. In the subsequent stage, data are acquired using several accelerometers to determine the shapes of modes. By fixing one accelerometer to a reference point (mid-point) and changing the positions of the other accelerometers, displacement data are collected, and modal shapes were derived by the calculation of relative displacements.

By calibrating finite element models with field measurements, this study shows how theoretical modelling can be used to understand how things work in the real world. Initial static analyses are conducted to check the system's capacity checks, like beam-column checks and tension checks with critical loads. By understanding the structure's dynamic responses in different modes, potential resonance conditions can be identified, ensuring the safety and comfort of pedestrians using the bridge. With the integration of seismic analyses, dynamic analysis can be conducted under different earthquake scenarios. Additionally, these studies can lead to long-term performance and sustainability of pedestrian bridges by serving as a model for early damage detection. With these contributions, the study not only serves as a model but also lays the foundation for many other steel pedestrian bridge studies.

2. LITERATURE REVIEW

The dynamic behaviour and vibration performance of bridges have been examined using analytical and experimental methodologies. Recent studies in computational tools and monitoring technology have allowed researchers to examine essential aspects influencing characteristics of bridges, including natural frequencies, mode shapes, and damping ratios. This review of the literature emphasises significant progress in the discipline, underlining the importance of finite element modelling and experimental methodologies. The reviewed works show the value of model calibration and propose design changes to ensure the comfort and safety of bridges by means of a comparison between analytical and prediction and experimental data.

2.1 Cable-Stayed Pedestrian Bridge

Jayaraman et al. [8] discussed how to design the main parts of cable-stayed pedestrian bridges, such as the main girder, pylons, support column, and cables, following established standards. In their study, they conducted capacity checks on the structural elements by including load calculations and wind load assessments affecting the bridge. The conclusion section emphasises that cable-stayed pedestrian bridges have safety, economic, and aesthetic advantages. Alocci et al. [9] conducted feasibility studies for a cable-stayed pedestrian bridge crossing over the Navicelli Canal in Italy. Their study provides detailed information about the bridge's construction phase, including the stages of the mounting plan. Several figures show the cross-sections of structural elements and the details of the connectors. As a result of structural analyses, they concluded that the bridge has feasible and economic advantages. Atmaca [10] conducted an optimisation study for cable sizes in a cable-stayed pedestrian bridge. With this study, the aim was to minimise cable weight, thereby reducing material costs and increasing structural performance. Pretensioning forces were increased, and the cross-section was reduced to reach optimum cables.

2.2 Analytical Approaches

Alocci et al. [9] carried out the analyses by creating a finite element model to check the feasibility of the steel pedestrian bridge. The available codes were checked for structural verification. Modal analyses were performed to determine the dynamic character of the bridge to assess the possible resonance risk. Atmaca [10] analysed the bridge by modelling it in SAP2000. In his study, he considered dead loads, pedestrian loads, and wind loads statically while addressing the earthquake load dynamically, conducting analyses for different load combinations. In the conclusion of the study, it was mentioned that the stress, vertical displacement of the deck, and horizontal displacement of the pylon in the improved cable-stayed system were all well below the maximum limits. This shows how important optimisation is. Polepally et al. [11] compared the natural frequencies for modes by modelling the cable-stayed bridge pylons as the A, H and inverted Y shapes using SAP2000 software and applied different earthquake scenarios that have already occurred. The smallest natural frequency was reached in an H shape, and the highest natural frequency was reached in an A shape. Within the scope of history analysis, the study applied earthquake scenarios and examined the displacement in the x and y directions on the deck and at the top of the pylon. Cheng et al. [12] emphasised that Artificial Neural Network (ANN) methods achieved higher accuracy and faster results compared to conventional approaches such as FEM methods and empirical methods. Their study included parameters such as the main span, the type of deck, and the support elements. ANN results were compared with experimental data, highlighting mass and stiffness as key factors in the determination of natural frequency.

2.3 Experimental Approaches

Aras [13] investigated the effects of vibrations under changing environmental conditions on the dynamic properties of a prefabricated and prestressed reinforced concrete pedestrian bridge. Vibration measurements on the bridge at different temperatures emphasised that the increase in ambient temperature caused a decrease in dominant frequencies. Human-induced vibrations have been determined to have no effect on dominant frequencies. The critical elements of cable-stayed bridges that carry high tension force are the cables, which are the elements affecting the stability and load-bearing systems of structures. Zhang et al. [14] have suggested that cable measurements can be more efficient and precise thanks to next-generation technological devices, and that with an increase in bridge spans, monitoring cable forces can become more practical and faster. Within the scope of cable health monitoring, Zhang et al. provided information on the applications of pressure gauge measuring methods, classical strain measurement, magnetic flux methods, vibration frequency methods, acoustic emission technology, fibre-optic sensors, and intelligent device monitoring methods, presenting their views for future health monitoring. Within the scope of health monitoring, Aras [15] examined the dynamic behaviour of the overpass pedestrian bridge located in İstanbul during and after its construction through modal tests. During the construction phase of the bridge, independent movement of girders was observed in the frequency values measured along the axes; elastomers controlled the dynamic behaviours. Measurements taken after the completion of the bridge showed that the girders of the bridge moved altogether. The impact of the two fundamental parameters, mass and stiffness, on the determination of frequency after completion of the structure has been emphasised, and it has been concluded that at higher frequencies, the contribution of stiffness is more effective than mass on a concrete slab. In the studies of examined literature, frequencies corresponding to peak points were mostly identified using the peak-picking method (PP) in ambient vibration tests. Magalhaes et al.

[16] compared results using different output-only identification techniques on the International Guadiana Cable-Stayed Bridge in their study. PP, Frequency Domain Decomposition (FDD), Covariance-Driven Stochastic Subspace Identification (SSI-COV), and Data-Driven Stochastic Subspace Identification (SSI-DATA) techniques are used. The PP and FDD methods can't tell the difference between modes with close frequencies, but the SSI-COV and SSI-DATA methods have better accuracy and can access both global and local modes.

2.4 Both Analytical and Experimental Approaches

Tubino et al. [17] determined the dynamic characteristics of the structures by analytical and experimental studies for two pedestrian bridges sensitive to human-induced vibrations in Italy, and the results were compared with the analytical approach by loading pedestrians modelled as harmonic loads on bridges modelled as elastic linear beams. It is emphasised that the natural frequencies of the bridge can enter resonance risk with vibrations during pedestrian walking. With the installation of Tuned Mass Damper (TMD) systems, vibration levels are reduced, and comfort is provided for pedestrians. The determination of the mode shapes, the dominant frequencies of the structure in different modes and the deformation shapes are important for understanding the dynamic character of the structure. Au et al. [18] explained the mathematical background of modal analysis theory and presented the natural frequencies and mode shapes with theoretical calculation methods on cable-stayed bridges. Modal measurements were carried out to verify the methods they used. The study concluded that the theoretical predictions aligned with the experimental measurements. For future analyses and long-term health monitoring, it is important to calibrate the finite element model with field data to achieve more realistic results. Ren et al. [19] created a 3D model of Qinzhou Cable Stayed Bridge using ANSYS software. Vertical modes, transverse modes and torsional modes were determined with the analytical model. In the other step, ambient vibration tests were conducted on the bridge deck and cables with a triaxial accelerometer. Power Spectral Density (PSD) determined the frequencies of the collected vibration data. Calculating the tension forces of the cables, which are critical structural elements, in different vibration modes, the "taut string" equation has been emphasised. The analytical model was calibrated with field data to provide a reliable basis, and it was emphasised that ambient vibration testing is a low-cost and effective solution. Gonilha et al. [20] conducted experimental measurements to determine the modal properties of reinforced concrete structures with Glass Fiber Reinforced Polymer (GFRP) and performed finite element modelling to validate experimental results. In their validation, it was observed that the results were largely consistent, with the experimental modal frequencies generally being at lower values. The differences that occurred were attributed to the assumptions and boundary conditions used in the modelling. It is strongly emphasised that one of the most important criteria in pedestrian bridges is pedestrian comfort. Ghetasi et al. [21] conducted studies on the serviceability of a 60-metre, 3-span continuous reinforced concrete slab supported by two longitudinal steel girders. In the first step of their study, a finite modal is created to obtain modal frequencies and mode shapes. They conducted ambient vibration tests to validate the dynamic characteristics of the model. By examining the dynamic responses of pedestrian groups walking at different numbers and frequencies, the study discussed the evolution of the pedestrian bridge in terms of service limit states in different codes. In their results, it was observed that the vertical frequencies of the bridge corresponded to the critical frequency ranges specified in the design guidelines. For the peak acceleration response, values were overestimated when using the equations of the current codes, and in this context, the studies suggested that existing design standards should be improved to achieve more reliable results in evaluating the vibration service performance of pedestrian bridges.

3. STUDIED BRIDGE

The bridge that was measured in the field is the Taşdelen Cable-Stayed Pedestrian Bridge. The bridge located at coordinates 41°01’36.58’ north and 29°13’47.79’ east is a busy bridge in terms of pedestrians crossing the Sile Road.

The structural elements of the bridge consist of 4 pylons, 2 edge beams, 12 tension stay cables, 4 end support columns, a steel plate deck, a concrete slab, and a staircase. S235 steel grade was preferred for all steel elements in the project. Figure 1 shows the front view of the existing bridge.

Figure 3.1: *Front View of the Taşdelen Cable-Stayed Pedestrian Bridge*

The bridge has three spans: L1 = 11.79 m, L2 = 28.62 m, and L3 = 12.66 m, for a total length of 53.07 m and a width of 1.9 m. Transverse beams, also known as floor beams and bracing, are located between two edge beams and have a steel deck plate with a thickness of 3 mm. A concrete class slab with a thickness of 8 cm and a class of C12/15 is located on the steel deck. The tension cables (stays) are used in a symmetrical manner, known as the harp model. The diameters of the cables from outside to inside are 16 cm, 13 cm, and 10 cm, respectively. The outermost cable length is 10.5 m, the middle cable length is 7.35 m, and the innermost cable length is 4.4 m. The innermost cables are fixed to the pylon at 9.15 m, the middle cables at 9.75 m, and the outermost cables at 10.35 m. The system has a total of four pylons with a height of 10.35 meters, and the four end support columns are located at the end. In the steel stairs, there are 4 columns with a height of 3 m. The height of the riser of all stairs is 16 cm, and the width of the stairs is 30 cm. The plan and front view, drawn in AutoCAD, are shown in Figures 3.2 and 3.3.

Figure 3.2: *Taşdelen Pedestrian Bridge—Front View*

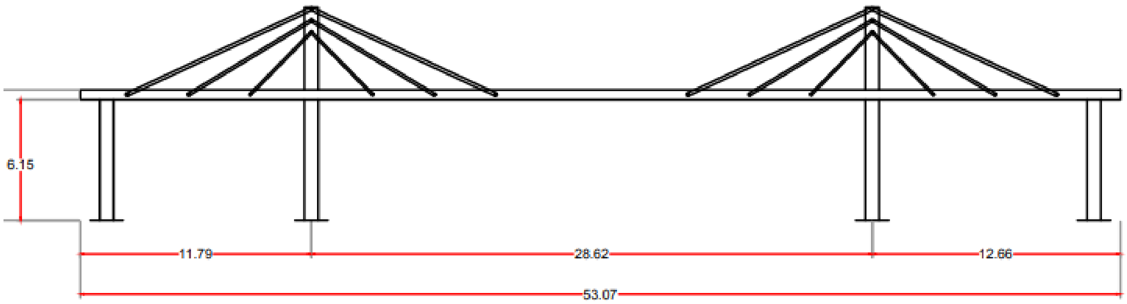

Figure 3.3: *Plan of the Existing Bridge*

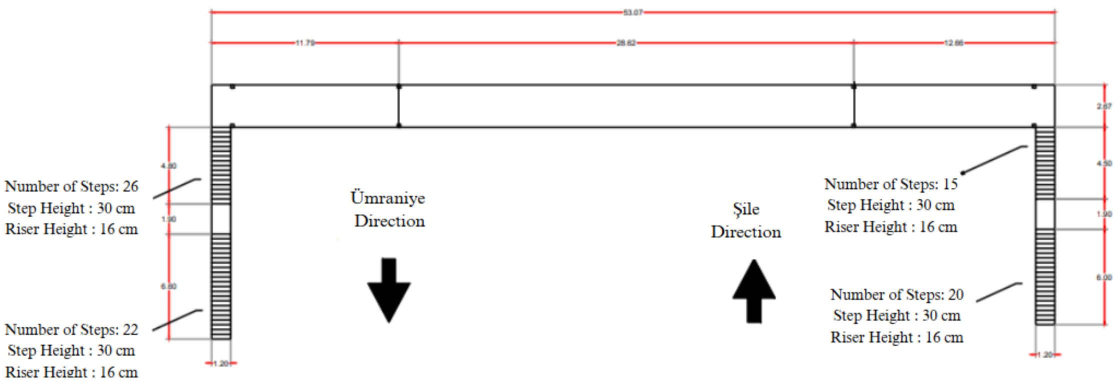

4. STRUCTURAL ELEMENTS AND SECTION PROPERTIES

Structural elements are the basic structural components that provide the safety, stability, and serviceability for the structure, forming the structural system. Understanding the load-carrying capacities of structural elements, and thus understanding the demand-capacity ratio correctly, plays an important role in structural safety, strength, and cost efficiency. In this context, the dimensions and cross-sectional properties of the structural elements were initially determined by field measurements. EN 1993-1-1 [4] was used to determine the properties of the section of all members.

Figure 4.1: *Notation for I profile according to EN1993-1-1[4]*

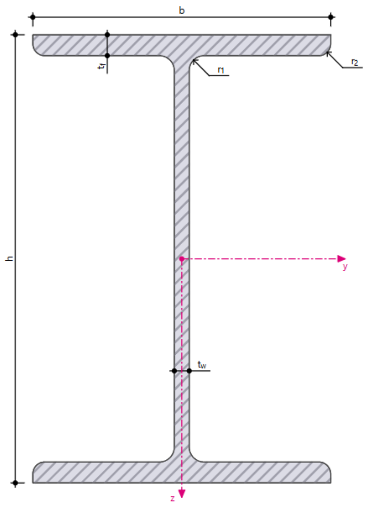

Figure 4.2: *Notation for Circular Hollow Section profile according to EN1993-1-1[4]*

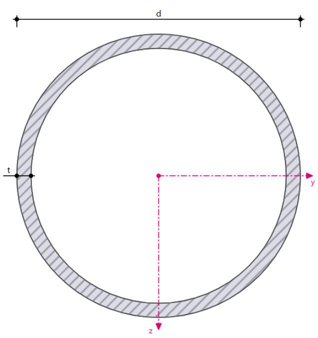

Figure 4.3: *Notation for Rectangular Hollow Section profile according to EN1993-1-1[4]*

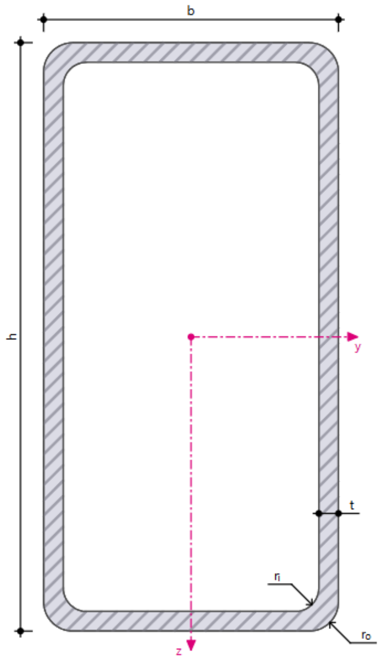

4.1 Vertical Members

The vertical structural elements of the bridge are divided into three types: pylons (the two main towers in the centre of the bridge are called pylons), end support columns, and stair columns. While the pylons carry both axial forces and moments, the other columns resist only the compressive force and transmit the load they receive from the cable to the ground. The bridge has four support columns at both ends and four additional columns at the staircase. The HEB700 with a steel plate as an built-up section was used for the main pylons and a 30X20 section for support columns and the stair's column. Figure 4.4 shows the vertical members of the bridge, and Tables 4.1 and 4.2 show the section properties of the columns. The load-bearing capacities of structural elements will be found using the section properties in the tables. The preliminary design part of the study will also include stability checks. The radius of gyration (r) calculated with the values from the tables will help to understand the slenderness behaviour of the compression members. Elastic section modulus (S) can be calculated by using the moment of inertia and height. The elastic bending strength capacities for the beams can be determined. In the preliminary design part of the study, the calculations will be presented in a detailed and comprehensive manner.

Figure 4.4: *Support columns, stair columns and pylons*

Table 4.1: *Properties of built up HEB700 section [1]*

Property	Value
Section	HEB700
Depth, h [mm]	700
Width, b [mm]	300
Web Thickness, t_w [mm]	17
Flange Thickness, t_f [mm]	32
Root Radius, r [mm]	27
Weight, m [kg/m]	240.5
Area, A [mm²]	93600
Moment of Inertia I_y ($\times 10^6$ mm^4)	4652
Moment of Inertia I_z ($\times 10^6$ mm^4)	1232

4.2 Horizontal Members

The horizontal elements consist of edge beams, transverse beams (cross beams), a thin steel deck plate, and a slab. External loads are primarily carried by the edge beams.

Table 4.2: *Properties of RHS 300×200/14.2 section [2]*

Property	**Value**
Section	RHS 300×200/14.2
Depth, h [mm]	300
Width, b [mm]	200
Wall Thickness, t [mm]	14.2
Outer Rounding Radius, r_o [mm]	21.3
Inner Rounding Radius, r_i [mm]	14.2
Weight, m [kg/m]	103.4
Area, A [mm²]	13177
Moment of Inertia I_y [$\times 10^6$ mm4]	158.3
Moment of Inertia I_z [$\times 10^6$ mm4]	83.28

The transverse beams connect the edge beams, which serve as the main load-bearing elements, ensuring a balanced distribution of loads. The thin steel plate and the concrete slab on top provide the walking surface for pedestrians, and they transfer their loads to the beams. These elements also enhance the rigidity of the bridge and help prevent Lateral-Torsional Buckling (LTB). Together, these elements form the bridge deck system, which plays a crucial role in distributing both lateral forces, such as wind and seismic loads, and vertical loads to the structural elements. This distribution enhances the overall stability.

Table 4.3: *Properties of HEB260 Edge Beam [2]*

Property	**Value**
Section	HEB260 (Main Girder)
Depth, h [mm]	260
Width, b [mm]	260
Web Thickness, t_w [mm]	10
Flange Thickness, t_f [mm]	17.5
Root Radius, r [mm]	24
Weight, m [kg/m]	93
Area, A [mm²]	11844
Moment of Inertia I_y [$\times 10^6$ mm4]	149.2
Moment of Inertia, I_z [$\times 10^6$ mm4]	51.35

Figure 4.5: *Edge beam, transverse beams and steel plate deck and bracings on the bridge*

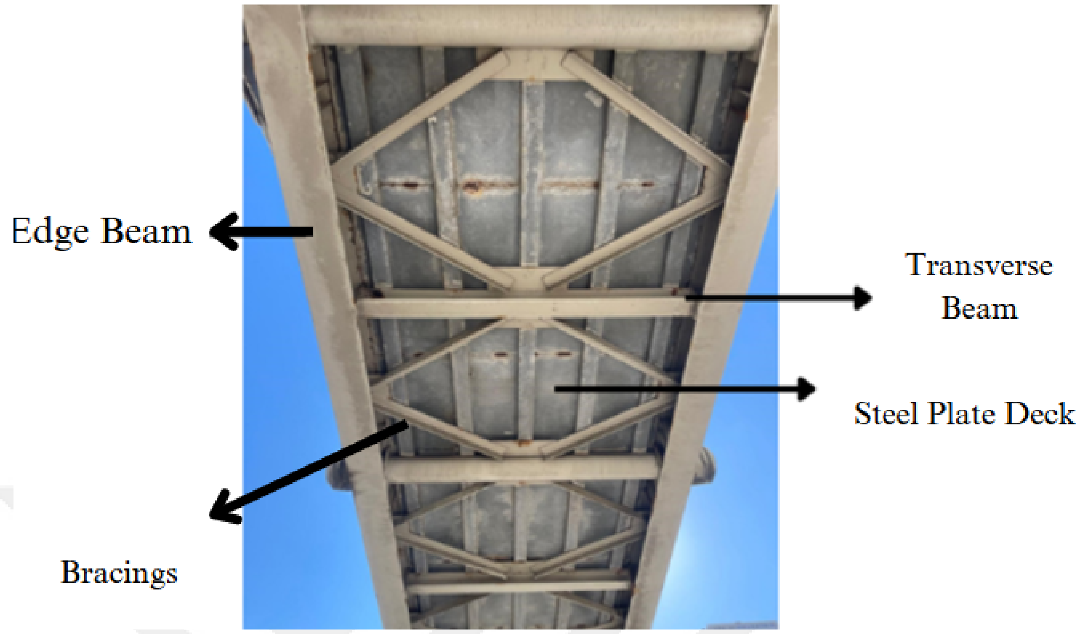

Table 4.4: *Properties of IPE 140 Transverse Beam [2]*

Property	**Value**
Section	IPE140 (Cross Beam)
Depth, h [mm]	140
Width, b [mm]	73
Web Thickness, t_w [mm]	4.7
Flange Thickness, t_f [mm]	6.9
Root Radius, r [mm]	7
Weight, m [kg/m]	12.9
Area, A [mm^2]	1643
Moment of Inertia, I_y [$\times 10^6$ mm4	5.412
Moment of Inertia, I_z [$\times 10^6$ mm4]	0.44

4.3 Tension Member

Stay cables are one of the main load-bearing components of the bridge. The cables are connected to the pylons and the deck system with pin connections and thus carry only the axial load. Tension cables transfer the load directly from the deck to the pylon. The cable stays of the bridge increase in diameter from the inside to the outside, as shown in Table 4.5. This is because the load-carrying capacity of the cable stays is directly proportional to their area. The outermost cable stays carry the majority of the load in the midspan of the deck system. Based on this scope, the span affects the outermost cable more. Capacity calculations are shown in detail in the preliminary design section.

Figure 4.6: *Tension cables on the bridge*

Table 4.5: *Properties of CHS Cables [2]*

Property	Inner Cables (CHS 101.6/3)	Middle Cables (CHS 139.7/3)	Outer Cables (CHS 168.3/3)
External Diameter, D [mm]	101.6	139.7	168.3
Wall Thickness, t [mm]	3.0	3.0	3.0
Weight, m [kg/m]	7.29	10.1	12.2
Area, A [mm²]	929	1288	1558
Moment of Inertia I [$\times 10^6$ mm4]	1.13	3.011	5.23

4.4 Bracings

Bracings are secondary structural elements that provide strength and stability to the structure. The columns and beams carry vertical loads, such as dead loads and live loads on the structure, while the bracing carries lateral loads, such as seismic loads and wind loads. There are two types of bracing on the Taşdelen bridge. Vertical bracing systems are located between the columns, and horizontal bracing systems are located between the main girders. X bracings are used vertically, while K bracings are used horizontally. Brockenbrough et al. [22] emphasised that X-bracing is an economical design but is weak in energy distribution during earthquakes. They recommended that seismically less active regions or short structures in an active region prioritise X-bracing. In this context, the X bracing used between columns for the Taşdelen bridge with a height of 6.15 m does not cause any problems. The Steel Bridge Design Handbook [23] emphasises the primary understanding of the buckling behaviour of I-profile beams. The I profile provides high moment capacity with weak torsion because of the thin web and wide flange. Under the bending moment, the beam may undergo lateral torsional buckling (LTB). However, bracings and concrete slabs work together as a rigid diagram in the bridge. In this case, they evenly distribute loads in the horizontal plane, and there is no lateral buckling because the girders' web and flange are supported by a rigid diaphragm.

Figure 4.7: *Horizontal bracing element: K-bracing (L50X5)*

5. NUMERICAL STUDIES

The main goal of this study is to build a finite element model of a real bridge and then test and confirm it with experimental studies and operational modal analyses. Before starting the experimental works, it is necessary to conduct analytical studies using SAP2000 software. Perform critical checks in this context, including the capacity and deflection of the bridge's structural elements. In the initial phase, static analyses were performed by applying loads to the model. The Load and Resistance Factor Design (LRFD) load combinations have been added to the finite element model so that it can be loaded in different scenarios. This process has been completed before the preliminary design phase. During the preliminary design, tension checks, compression checks, and beam and beam column checks were conducted. In contrast to the preliminary design, the overall design part looked at the overall structural capacity instead of element-based evaluation. This meant that the load combinations in the finite element model were used in more detail with wind loads. Since no instances of capacity exceedance were observed, the model was deemed structurally safe according to the analytical study. After validating the modal with static analyses, we conducted a modal analysis, also known as a dynamic analysis, using SAP2000. This stage ensured the determination of the dynamic behaviour of the bridge through analytical studies.

5.1 Theoretical Basis of the Finite Element Method

The finite element method (FEM) is a numerical method used to solve engineering problems [24]. It helps in analysing structural systems based on complex geometric shapes, material properties, and various applied loads. By performing analyses, you can look at the strength of the structural elements and how they deform. You can also find out how the structure changes over time with dynamic analyses, like modal analysis and nonlinear time history analysis. Design optimisation can strengthen structural elements, and the use of the best materials can save you money [25]. The different types of analyses can look at the strength and deformation patterns of the structure's parts. Dynamic analyses, like modal analysis and nonlinear time history analysis, can show how the structure changes over time. Understanding the finite element method forms the basis for numerical studies. SAP2000v.20 [1] finite element software, which offers a single user interface to perform modelling, structural analysis, design, and reporting.

In the first part of the study, dimensions and material properties of structural elements found on the site were modelled in SAP2000. A major goal of the study is to model the bridge structural analysis as accurately as possible to match experimental results. In the design part, loads were added to the bridge model, and static analysis and capacity checks were performed. Experimental modal analysis will be used to confirm the dynamic character found by modal analysis, and if needed, calibration will be used to update the model.

With the Finite Element Method (FEM), a stiffness matrix representing the behaviour of structural elements under external forces considering their geometry and material properties is easily constructed for complex structures. This matrix expresses the resistance of the element to external forces and its resistance to deformation. The system divides each element into a finite number and connects them to nodes. After finding the local stiffness matrix for each element separately, the global stiffness matrix is obtained. Applying the boundary conditions leads to the solution. Complex structures with too many nodes make manual solutions nearly impossible, necessitating the use of software tools like SAP2000.

The writing of the stiffness matrix is one of the critical points in the basis of Finite Element Analysis (FEA). The stiffness matrix is related to the properties and geometry of the material. The matrix, the relationship between the applied loads to the structure and the displacements at the nodal points, is written in Equation 5.1

$$\{\mathbf{F}\} = [\mathbf{K}] \cdot \{\mathbf{U}\} \tag{5.1}$$

The first step involves finding the local stiffness matrices of the elements. The cables in the bridge studied are elements that carry only axial forces. They do not carry moments and shear forces. For a 2D truss element, there are a total of 4 free degrees. (2N x 2N). N is the number of nodes in the elements. The stiffness matrix of the cables is shown in Equation 5.2.

$$[k]_{\text{local}} = \frac{EA}{L}\begin{bmatrix} 1 & 0 & -1 & 0 \\ 0 & 0 & 0 & 0 \\ -1 & 0 & 1 & 0 \\ 0 & 0 & 0 & 0 \end{bmatrix} \tag{5.2}$$

Where E is the modulus of the elastic section, A is the cross-sectional area, and L is the length of the element.

The transformation matrix participates in the conversion of local coordinates to global coordinates. Since the transformation matrix is not a square matrix, it cannot be inverted and must be expanded. Equation 5.3 displays the 4x4 square expanded transformation matrix T. [24]

$$T = \begin{bmatrix} c & s & 0 & 0 \\ -s & c & 0 & 0 \\ 0 & 0 & c & s \\ 0 & 0 & -s & c \end{bmatrix} \tag{5.3}$$

where $c = \cos\theta$ and $s = \sin\theta$

Equation 5.4 shows how to write the global stiffness matrix, and Equation 5.5 represents the global stiffness matrix.

$$[k]_{\text{global}} = T^T [k]_{\text{local}} T \tag{5.4}$$

$$[k]_{\text{global}} = \frac{EA}{L} \begin{bmatrix} c^2 & cs & -c^2 & -cs \\ cs & s^2 & -cs & -s^2 \\ -c^2 & -cs & c^2 & cs \\ -cs & -s^2 & cs & s^2 \end{bmatrix} \tag{5.5}$$

The beams carry shear force and moment in the matrix formulation, unlike truss members. The axial forces are neglected. Beam elements have a total of 4 degrees of freedom in 2D dimensions. Each node has transverse displacement (v) and 1 rotational freedom (θ). Figure 5.1 shows the forces, vertical displacements, and rotational displacements of the beam.

Figure 5.1: *Beam Member*

Euler-Bernoulli beam theory is used when writing the stiffness matrix of the beam element. The derivation of displacement is equal to the rotation. The Euler-Bernoulli stiffness matrix is shown in Equation 5.6.

$$K = \frac{EI}{L^3}\begin{bmatrix} 12 & 6L & -12 & 6L \\ 6L & 4L^2 & -6L & 2L^2 \\ -12 & -6L & 12 & -6L \\ 6L & 2L^2 & -6L & 4L^2 \end{bmatrix} \tag{5.6}$$

The stiffness matrix of the frame elements is obtained by combining the behaviour of the truss and beam matrices. As shown in Figure 5.2, horizontal displacement, vertical displacement, and rotation at one node have a total of 6 degrees of freedom (3D).

Figure 5.2: *Frame Member*

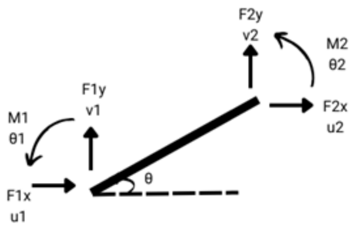

By combining the matrices of truss member and beam member in 6x6 format, the local stiffness matrix is written as shown in Equation 5.7

$$k_{\text{local}} = \begin{bmatrix} \frac{EA}{L} & 0 & 0 & -\frac{EA}{L} & 0 & 0 \\ 0 & \frac{12EI}{L^3} & \frac{6EI}{L^2} & 0 & -\frac{12EI}{L^3} & \frac{6EI}{L^2} \\ 0 & \frac{6EI}{L^2} & \frac{4EI}{L} & 0 & -\frac{6EI}{L^2} & \frac{2EI}{L} \\ -\frac{EA}{L} & 0 & 0 & \frac{EA}{L} & 0 & 0 \\ 0 & -\frac{12EI}{L^3} & -\frac{6EI}{L^2} & 0 & \frac{12EI}{L^3} & -\frac{6EI}{L^2} \\ 0 & \frac{6EI}{L^2} & \frac{2EI}{L} & 0 & -\frac{6EI}{L^2} & \frac{4EI}{L} \end{bmatrix} \tag{5.7}$$

The transition from local coordinates to global coordinates differs according to the transformation matrix in Equation 5.3. Unlike the truss members, it incorporates rotation into the calculation. Equation 5.8 displays the new transformation matrix.

$$T = \begin{bmatrix} c & s & 0 & 0 & 0 & 0 \\ -s & c & 0 & 0 & 0 & 0 \\ 0 & 0 & 1 & 0 & 0 & 0 \\ 0 & 0 & 0 & c & s & 0 \\ 0 & 0 & 0 & -s & c & 0 \\ 0 & 0 & 0 & 0 & 0 & 1 \end{bmatrix} \tag{5.8}$$

$$[k]_{\text{global}} = T^T [k]_{\text{local}} T \tag{5.9}$$

5.2 Modeling

The physical structural elements in the bridge model are represented by objects. The first step involves drawing the column, beam, and brace elements using line objects, also known as frame objects. The stays used in the bridge are modelled in the same way since they have a tube cross-section. The existing bridge models the concrete slab, where pedestrians move on the deck, as an area object or shell element. At the beginning of the model, the pylon, beam, and stays of the bridge are modelled in 2D as line objects.

Figure 5.3: *2D line model of the bridge*

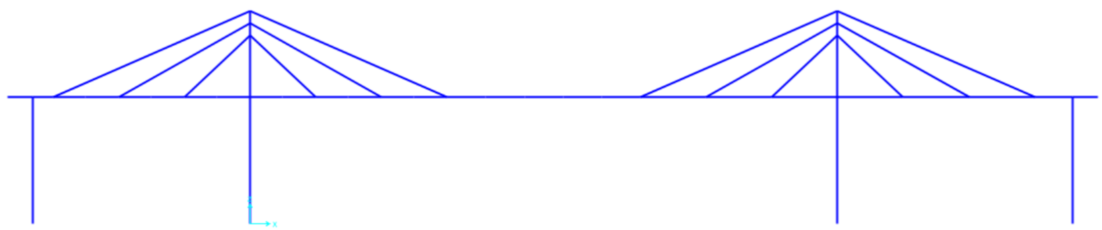

Each structural element in the model has its local coordinate system, and since the whole model is defined in the global coordinate system, it is passed to the global system by vector cross products. Local systems are represented as 1, 2, and 3, while the global system is represented as x, y, and z. In the local system, the right-hand rule applies to the longitudinal direction; the thumb is 1 (red). The other fingers indicate direction 2 (green), while the palm indicates direction 3 (blue). In Figure 5.7, the green arrow corresponds to the height of the section, while the blue arrow corresponds to its width.

Figure 5.4: *Pylon's local axis*

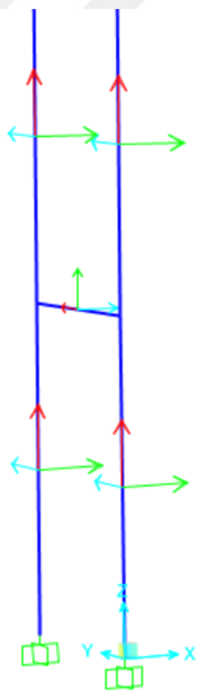

After the frame line geometry is drawn, section properties are assigned to the objects to define the physical elements (structural elements). Frame sections are the material and geometrical properties that define the sections of the elements. During the field investigations, the section properties of the bridge elements were obtained, and the sections conforming to the European standards were imported to SAP2000 and assigned to the model. Additionally, the built-up pylon section was designed using the section designer in SAP2000.

Figure 5.5: *Section Properties*

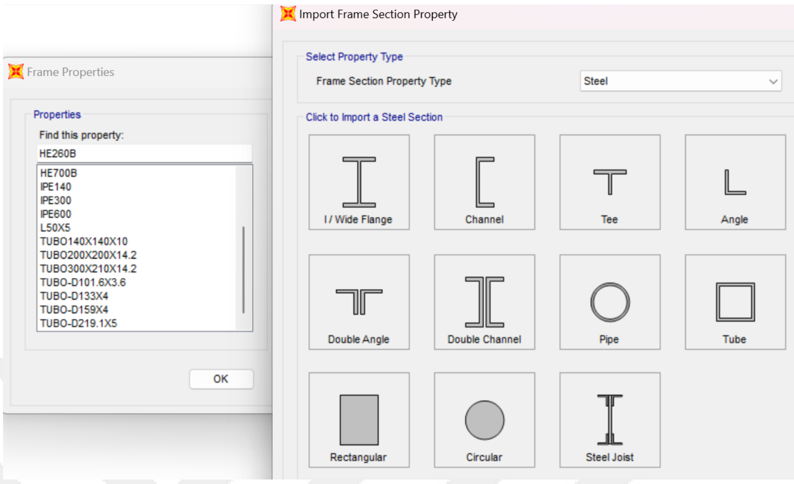

The joints to be used in the bridge model are the connection points of the elements. Each joint has degrees of freedom to determine how the connected element will move (translation and rotation). With joints, support conditions, and connections defined in the model. Pylons and columns use fixed support, restricting all possible movements. Nodes, apart from the connection between stays, work as automatic rigid connections.

Figure 5.6: *Bridge's Fixed Support*

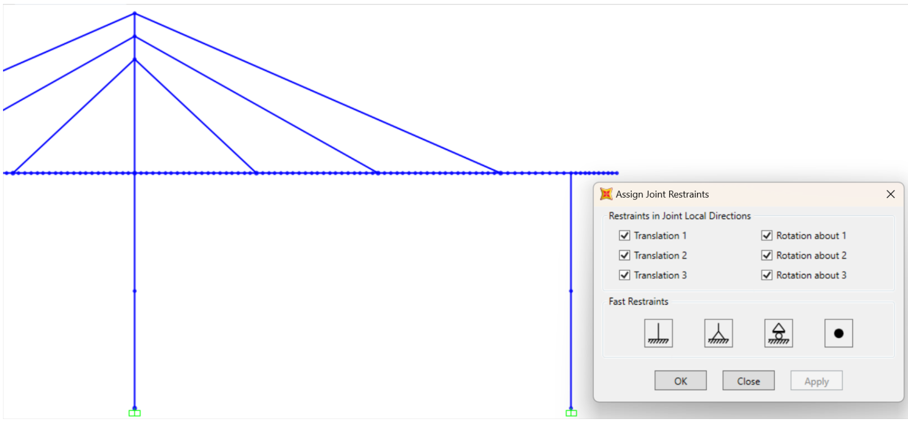

The observation revealed a pin-pin connection between the stays on the bridge.

Based on this, moment release was performed at both ends of the stays so that the stays can only carry axial load in the model.

Figure 5.7: *Releases Applied to Stays*

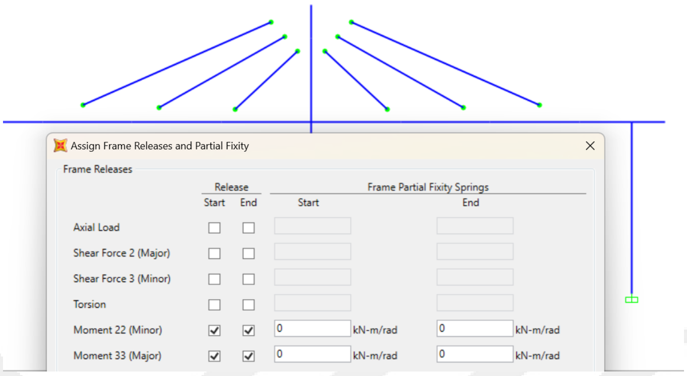

After drawing the 2D model in the x-z direction, the model is duplicated at a distance of 1.9 m on the y-axis. When the model was switched to the three-dimensional finite model, the bracing and transverse beams in the y-axis were added to the model, and the deck model was completely formed. On the deck, the steel plate was defined as a shell element and assigned to areas. Since the C12/15 concrete slab on the steel plate is not rigid, it has been neglected, and only its weight has been calculated and added as additional mass to the dead load. The bridge system was added to the model in order to model the model as close as possible to the existing bridge.

Figure 5.8: *3D Model of Existing Bridge*

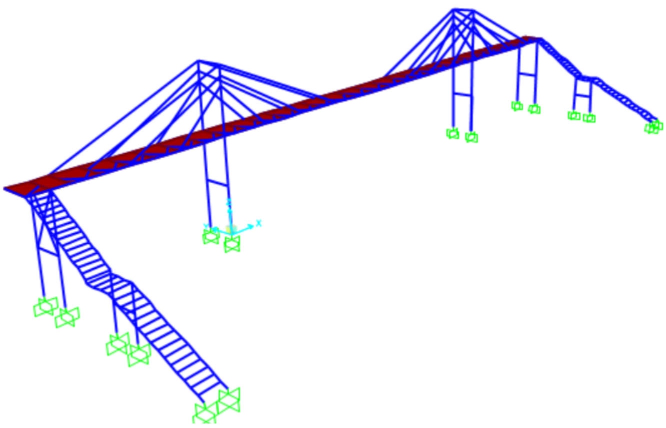

5.3 Loads

The limit state is an important principle that defines the performance criteria points under different load combinations in structural design. In this part, dead loads, live loads, and wind loads acting on the structure are calculated and assigned to the finite element model. These loads are multiplied by various load factors to provide a safe design for possible uncertain conditions [3] [26]. The loads multiplied by the coefficients are compared with the capacities of the structural elements against different scenarios by creating different load combinations. Resistance factors multiply the calculated capacities as an additional safety measure. The design part, following AASHTO LRFD [3], takes into account two main limit states. The first, the strength limit states, focuses on the adequate resistance of a structure against collapse in the presence of loadings, whereas the serviceability limit states focus on the suitability of the structure for use without losing its bearing capacities.

The preliminary design part of the study assigns vertical and horizontal loads with a combination and compares them with the capacities of the calculated structural elements. Tension checks for cables, compression checks and beam column checks for pylons and beam checks for the edge beam were performed, and the strength limit states were compared. Wind loads were assigned to the pylons and the main girder of the bridge statically. The wind load calculation is detailed in the load section.

5.3.1 Dead Load

Dead loads are constant loads that act continuously on the bridge and do not change over time. These loads consist of the weight of the bridge itself and the fixed components on it. Beams, pylons, cables, steel plate decks, concrete slabs, and railings create dead loads due to their own weight. SAP2000 automatically calculates the self-weight of the modelled structural elements. Additional dead loads not added to the model (railings) are manually calculated and assigned to the model. The calculation of the dead load of the concrete slab, the density of concrete C12/15 (2500 kg/m³), is multiplied by the thickness of the slab (0.08 m), and the dead load is found by unit conservation and is expressed in the following equations in the appendix. B.

Multiplied by the depth of the bridge (1.9m) to be able to act as a distributed load (kN/m) and to be equally distributed to the two edge beams.

Dead load values for bridge railings are given in EN1991-2. It is recommended to take 2.5 kN/m for concrete support of the safety barrier and 0.638 kN/m for steel railings. For a safer design, a distributed load of 3 kN/m (railing, concrete slab and steel plate) is entered into the model.

Figure 5.9: *Dead Load on the Bridge*

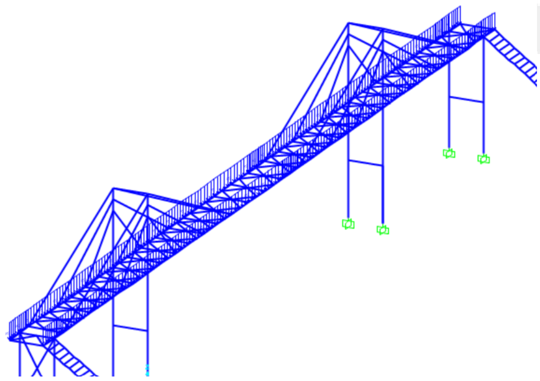

5.3.2 Live Load

The live loads acting on the bridge refer to the loads that changed over time on the bridge. According to the AASHTO LRFD Bridge Design Specification [3], live loads recommend the use of a distributed load of 4.10 kN/m^2 in bridge design for pedestrian and bicycle use only. Bicycle and human movements are referred to as pedestrian live loads, and dynamic loads are not considered.

For a safe design, a pedestrian live load of 5 kN/m^2 is preferred, and this is multiplied by width (1.9 m). The total load is distributed to two edge beams is 4.75 kN/m

Figure 5.10: *Live Load on the Bridge*

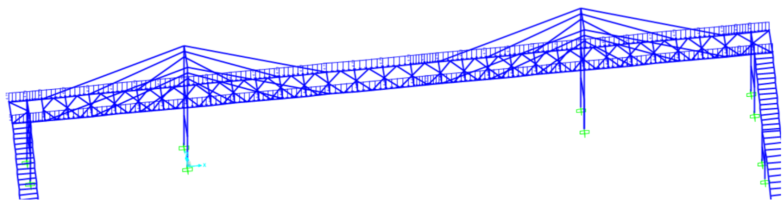

5.3.3 Wind Load

Cheng et al. [27] analysed the ultimate bearing capacity of the Lu Pu Steel Arch Bridge constructed in Shanghai under static wind loads. They considered different load combinations by loading their bridge in accordance with the design regulations used in their country. They pointed out that the carrying capacity decreases as the wind load increases. Small loads on the Taşdelen Cable-Stayed Pedestrian Bridge caused the system to behave elastically. The study of the Lu Pu bridge also looked at nonlinear effects.

Yin et al. [28] investigated the dynamic response of a long-span bridge under the combined effect of wind and wave loads. Aerodynamic force coefficients from tests in a wind tunnel and a wave channel were used to figure out the wind loads acting on the pylons and deck. In the study, experimental data was compared with numerical simulations performed in the finite element model on ANSYS, and validation was carried out.

Zdravkov [29], has modelled different types of bridge sections and determined aerodynamic coefficients by Computational Fluid Dynamics (CFD) analysis. Zdravkov examined the behaviour of each girder against wind loads by increasing the number of main girders. The wind load affected the beams located on the windward side the most, and their aerodynamic coefficients were found to be higher. The aerodynamic coefficients of the beam on the leeward side were found to be very small or negative values. Analysis of the results revealed that steel girder bridges had higher vertical aerodynamic coefficients. In other words, steel bridges generate greater lifting force. The heavier reinforced concrete sections reduce the effect of these forces. In this study, steel bridges were exposed to more wind loads than concrete bridges. The main reasons for this are the differences in cross-section and weight. Due to the thinner steel sections, more turbulence occurs. In steel sections, airflow can be separated more easily, and this creates a separation effect, i.e., vortex formation. This leads to the creation of variable wind loads. Analysis of their dynamic behaviour reveals that steel structures are more prone to wind-induced vibration due to their lighter weight. Dampers and additional weights can reduce vibration.

Suangga et al. [30] compared the wind loads acting on a truss bridge with the Standar Nasional Indonesia (SNI) and the AASHTO standards. The comparison also highlighted the differences between the regulations used in previous years and the current ones. Their findings demonstrated that the new and current regulations outperformed the previous ones in terms of wind load values. In SNI-2005, it was stated that wind speeds are constant and do not change with height, while SNI-2016 underlines that wind speeds increase with height. Based on this study, new and updated regulations have calculated higher wind loads to ensure that bridges are more resistant to wind loads. Bridges that are currently active and bridges built in the past years should be checked.

TS EN 1991-1-4 [5] performs calculations for the cable-stayed pedestrian bridge after examining various studies in the literature. The main wind pressure formula is given in equation 5.10.

$$q = \frac{1}{2}\rho v^2 C \tag{5.10}$$

Where v is the wind speed, p is the density of air, and C is the wind load coefficient. For safe design, a wind speed as high as 40 m/s (144 km/hr.) is accepted. C value is equal to the product of Ce and Cf values; Ce is obtained from figure 22, and Cf is 1.3 for normal bridges.

Figure 5.11: *Graph of Ce with increasing Height [5]*

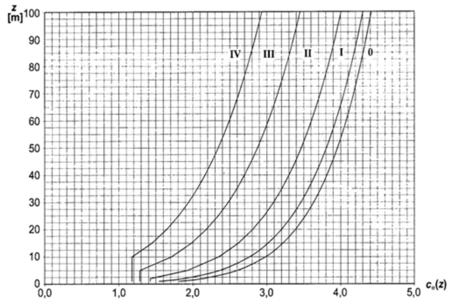

The value calculated shall be loaded uniformly and horizontally on the girder and pylons of the bridge. The axial loads on the bridge are not included in the study. In section 8 of the Turkish Standard [31], while the recommended speed value for design is 23 m/s, 40 m/s used in the study is too high. It is emphasised that for bridges with a span of less than 40 m, applying a dynamic load is not necessary.

Figure 5.12: *Wind Load on the bridge*

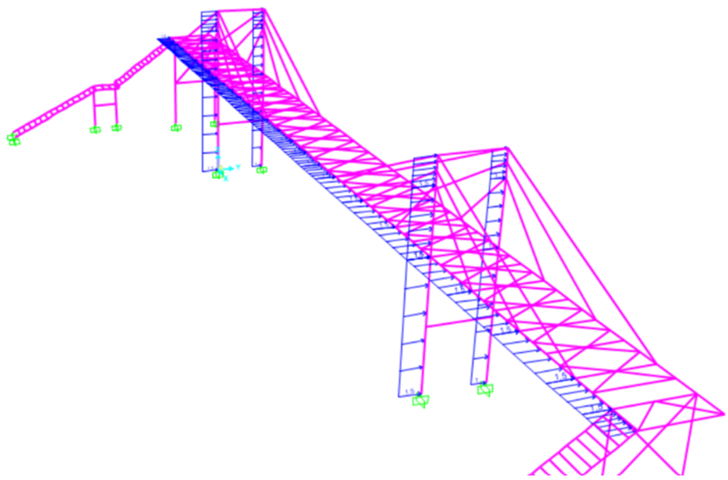

5.4 Load Factors and Load Combinations

The load combinations denote the various loads that the structure will encounter and the methods used to account for them. These loads are multiplied by certain factor values to make the design safer and more economical. The general idea is that the loads acting on the bridge are not below the limit state in terms of safety even under the worst-case scenarios.

The principles known as limit states define the points in structural design where certain performance criteria fail to be met. Structural design controls not only the strength but also the serviceability of the structure. In strength combinations, critical loads in terms of bearing capacity and stability are reached with the highest factor values, while in service limit states, the user's comfort with the structure is considered. Therefore, in order to see more realistic effects of the loads, they are multiplied by 1 as a factor.

$$\sum \gamma_i \cdot F_i \leq \phi R_n \tag{5.11}$$

In Equation 18, F_i represents the different loads acting on the bridge (dead load, live load, wind load), while γ_i represents the load factors. The right-hand side of the equation shows the nominal resistance R_n, and ϕ represents the resistance factor.

The load combinations used in the study are listed below. [3]

- **Strength 1** - Simple load combination without wind .
- **Strength 3** - Combination where the bridge is exposed to a wind speed of at least 25 m/s (wind factor is the highest).
- **Strength 5** - Combination of normal use of the bridge and inclusion of at least 25 m/s wind effect. (Preferred combination in the preliminary design part of the study)

- **Service 1** - Combination where wind and other loads are used with nominal values. Combination where realistic effects of loads are analysed.

Table 5.1: *Load Combinations [3]*

Load Combination	Equation
Strength 1	$1.25DL + 1.75LL$
Strength 3	$1.25DL + 1.40WL$
Strength 5	$1.25DL + 1.35LL + 0.4WL$
Service 1	$1.00DL + 1.00LL + 0.3WL$

5.5 Static Analysis of Existing Bridge

In the first stage of the static analysis, load combination 5 was used to determine the axial forces, shear forces, and moments applied to the elements. The static analysis was performed using SAP2000, with red representing pressure and blue representing tension in the figures.

When examining the axial force diagram, it can be seen that the cables carry tensile forces as expected, and due to the span, the outermost cable carries more force than the other cables. In response to the horizontal forces on the cables, compressive forces have developed in the beams to balance these forces. The loads from the deck are transferred to the pylons, where high compressive forces are observed in Figure 5.13.

Figure 5.13: *Axial Force Diagram*

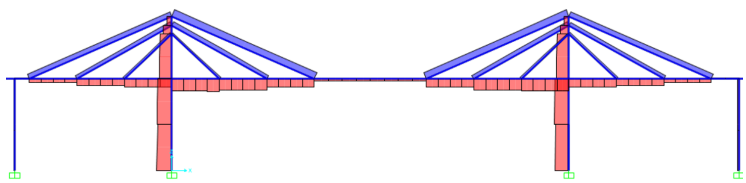

The dead load, live load, and wind load acting on the deck affecting the existing bridge have created shear forces in various elements of the load-bearing system. These loads, directed to the pylons by the cables, cause shear forces, especially in the pylons and the main span. The cables, on the other hand, only carry axial loads (both ends are pins), so no shear forces or moments are generated.

Figure 5.14: *Shear Force Diagram*

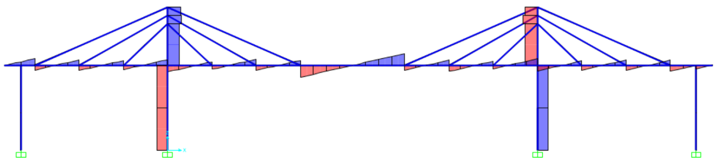

When the moment diagram is examined, it is determined that there is a moment in the pylons and the edge beams of the middle span. This means that these pylons are beam-column elements (carrying both axial load and moment) in the structure.

Figure 5.15: *Moment Diagram*

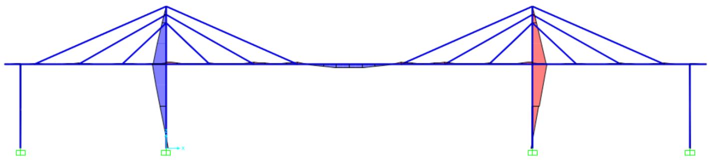

When examining the diagram, it can be observed that the beams between the pylon and the cable carry axial loads, while the beam elements at the centre carry moments. This means that the elements between the cables and the pylon act as truss systems and only carry axial loads.

The 3D static analysis was performed using SAP2000 software in the finite element model. The AISC 360-16 [31] standard was used for the analysis in the program. Although both LRFD and ASD are available in this standard, the LRFD method was preferred.

The contour map shown next to the bridge represents the applied load/capacity ratio of the elements. In the design section, the maximum load on structural elements from different load combinations is determined and divided by the capacity. When examining the figure, it can be seen that the structural elements between the outermost cables operate at a capacity between 0 and 0.5, while the outermost cables operate at a capacity between 0.5 and 0.7.

Figure 5.16: *Overall Static Analysis of the Bridge*

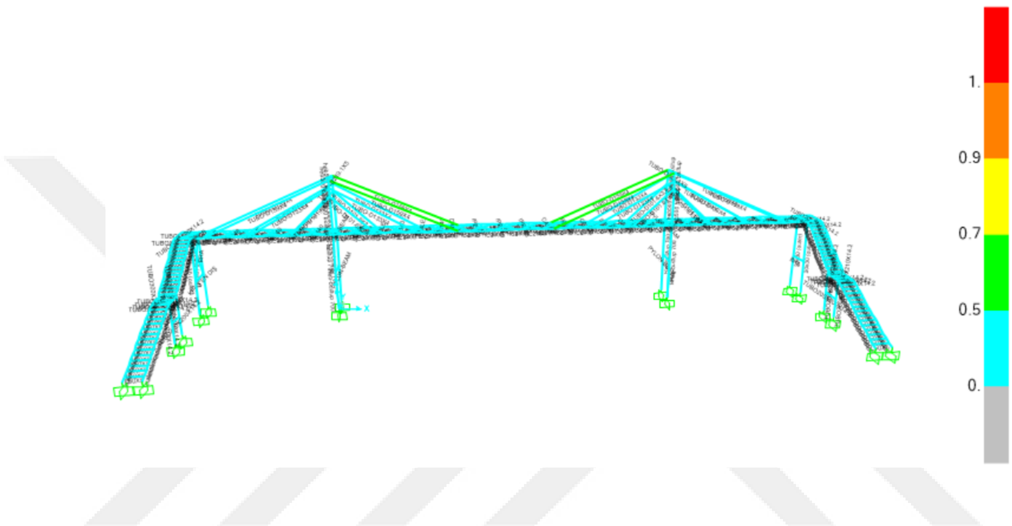

Table 5.2: *Demand/Capacity Ratios of Structural Elements*

Element	Demand/Capacity Ratio
Pylon	0.11
Edge Beam	0.25
Cable	0.526

6. DYNAMIC ANALYSIS

Dynamic analysis is an essential part of understanding how structures behave and determining how they react under time-varying dynamic loads, including earthquakes, wind, traffic, and vibration. The study intends to determine the behaviour of the structure with respect to displacement, velocity, acceleration, and internal forces.

Due to the external loads acting on the structure, elastic potential energy and kinetic energy are stored in the structure. These two energies periodically transform into each other to form oscillatory motion. Oscillatory motion is referred to as vibration. This study applied free vibration to determine the dynamic character of the bridge with modal analysis. The dynamic characteristics of the structure include its natural frequencies, mode shapes, and responses.

The study's analytical section included both static and dynamic analyses. The key distinctions between the two analyses are outlined and discussed in detail.

- In contrast to static analysis, which considers constant loads (not changing with time), such as dead loads and live loads, dynamic analysis considers loads such as earthquakes, traffic, etc., which change with time and create acceleration and inertia effects. In the real bridge study, the wind load was considered statically for ease of calculation

- While static loads act on the structure continuously, dynamic loads can be instantaneous, such as earthquakes, or can be modelled periodically, such as vehicles passing over the bridge.

- The equation of equilibrium is used in static analysis, while the equation of motion is used in dynamic analysis.

6.1 Mathematical Formulation of Dynamic Systems

In a Single Degree of Freedom (SDOF) system, the system is modelled with a single mass, a single spring, and a single damper, while in Multiple Degree of Freedom (MDOF) systems, it is modelled with multiple masses, springs, and dampers. In real applications, MDOF is more complex and more precisely reflects the actual system behaviour. It uses matrix equations to solve the analyses. The dynamic analysis chapter begins with an explanation of single stiffness systems. This allows us to understand the basic logic of MDOF systems. Analysing an MDOF system involves breaking it down into several simpler SDOF systems, each of which represents a distinct mode. The analysis uses modal analysis to obtain a separate natural frequency and mode shape for each mode.

6.1.1 *Single Degree Of Freedom*

When dynamic systems are modelled, the mass-spring-damper model is used. This model is a simplified system that helps us understand how real-world systems vibrate and move. Firstly, the basic principle of working with the single-degree freedom system is presented, and then the multi-degree freedom system is presented to better analyse the bridge. For the basic mathematical formulas used in the dynamic analysis part, Dynamics of Structures: Theory and Applications to Earthquake Engineering [6] was followed.

Figure 6.1: *Mass-Spring-Damper Model for SDOF*

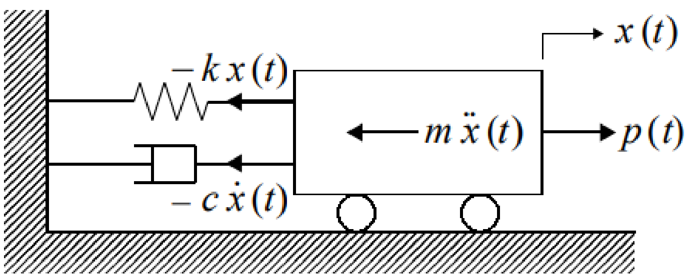

The system represents the spring force (the elastic recall force) as kx(t). The '-' sign at the beginning indicates that the resistance force ($F_r = kx$) is always in the direction to stabilise the motion.

The process in which the amplitude decreases continuously is called damping. The damping force ($F_d = c\dot{x}$), like the resistive force, is always in the direction opposite to the motion. The damping coefficient depends on stiffness, mass, and the damping ratio. Since welded and bolted fasteners were used in the real bridge, a damping ratio of 1$\%$ was used according to AASHTO LRFD [3].

Equations show the external force p(t) acting along the axis and its representation using Newton's second law.

$$p(t) - F_s - F_d = m\ddot{u} \tag{6.1}$$

$$m\ddot{u} + c\dot{u} + ku = p(t) \tag{6.2}$$

Equation (6.2) shows the general equation of motion. The main scope of the study is to ensure that the natural frequency values obtained from the analytical study and the natural frequency values obtained from the field investigations are as close as possible to each other. The natural frequency was directly reached by modal analysis, and the undamped free vibration section is the basis of the modal analysis.

6.1.2 Multi Degree Of Freedom

In order to understand the theory and principles of multi-degree-of-freedom systems, the system is idealised in 2D, and a simplified mass-spring-deflection model with only horizontal translational motion is used to explain the basic principles. In other words, since the real bridge has a large number of nodes and 6 degrees of freedom in each node, the SAP2000 software program was used for the analysis of the complex bridge. The system shown in the figure has a total of 2 masses, i.e., 2 nodes. Each node has only 1 degree of freedom horizontally, and a total of 2 degrees of a freedom system model is shown in Figure 8.1.

Figure 6.2: *a) Mass-Spring-Dampin Model for MDOF b) Free-Body Diagrams [6]*

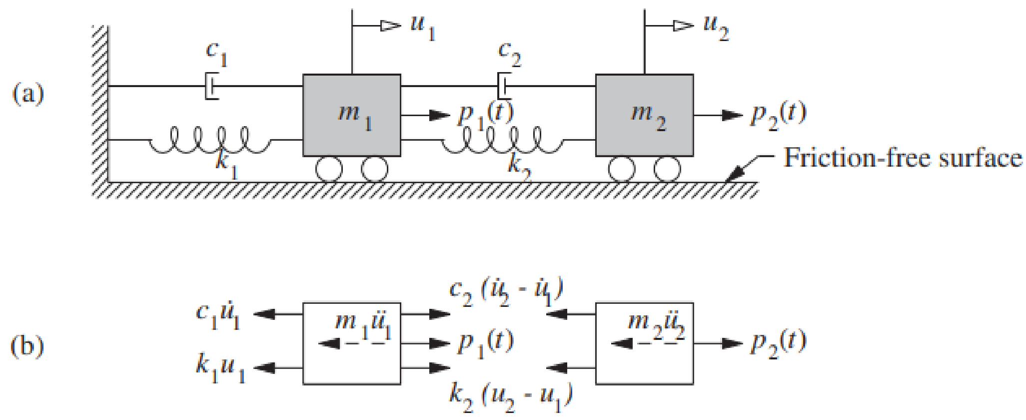

Thanks to the idealised model, the matrix formation required to analyse complex structures is shown in its simplest form.

$$\begin{bmatrix} m_1 & 0 \\ 0 & m_2 \end{bmatrix} \begin{bmatrix} \ddot{u}_1 \\ \ddot{u}_2 \end{bmatrix} + \begin{bmatrix} c_1 + c_2 & -c_2 \\ -c_2 & c_2 \end{bmatrix} \begin{bmatrix} \dot{u}_1 \\ \dot{u}_2 \end{bmatrix} + \begin{bmatrix} k_1 + k_2 & -k_2 \\ -k_2 & k_2 \end{bmatrix} \begin{bmatrix} u_1 \\ u_2 \end{bmatrix} = \begin{bmatrix} p_1(t) \\ p_2(t) \end{bmatrix} \tag{6.3}$$

6.2 Free Vibration

6.2.1 Undamped Free Vibration

Free vibration is the condition where the system vibrates with its own internal forces when the force p(t) is 0. This study will base its modal analysis on undamped (c=0) free vibration.

In general, a harmonic function is the best way to solve the equation of motion of a system with one degree of freedom and no damping.

$$u(t) = A\cos(\omega_n t) + B\sin(\omega_n t) \tag{6.4}$$

The coefficients A and B in the formula change according to the initial conditions. While the function gives A at $u(0)$, the first derivative of the function gives B at $\dot{u}(0)$.

$$u(t) = u_0 \cos(\omega_n t) + \frac{\dot{u}_0}{\omega_n} \sin(\omega_n t) \tag{6.5}$$

When the second derivative of Equation (5.48) is taken and solved for ω_n, the natural frequency formula is obtained:

$$\omega_n = \sqrt{\frac{k}{m}} \tag{6.6}$$

It has been verified that the 2 main parameters for the natural frequencies to be obtained in modal analysis are stiffness and mass. In the scenario where the natural frequency data is to be collected in the field and analytical results cannot match, changes will be made to these two parameters.

6.2.2 Damped Free Vibration

In contrast to undamped free vibration, damping is involved in this section. Damping reduces the vibration energy of the system over time and brings it to equilibrium. When equation 5.47 is divided by m:

$$\ddot{u} + 2\zeta\omega_n \dot{u} + \omega_n^2 u = 0 \tag{6.7}$$

In equation 5.51, the damping coefficient c is written in terms of the damping ratio, and the connection between them is given below.

$$\zeta = \frac{c}{2m\omega_n} = \frac{c}{c_{cr}} \tag{6.8}$$

An underdamped system with a dumping ratio between 0 and 1 was studied. Which decreases exponentially with time due to the $e^{-\zeta\omega_n t}$ factor. The representation of a general solution

$$u(t) = e^{-\zeta\omega_n t} \left(A\cos(\omega_d t) + B\sin(\omega_d t) \right) \tag{6.9}$$

ω_d is the damped natural frequency. When the damping ratio is 0, the damped natural frequency is equal to the natural frequency, and this is the undamped free vibration system. When the damping ratio is increased, the oscillation in the system decreases more quickly.

$$\omega_d = \omega_n \sqrt{1 - \zeta^2} \tag{6.10}$$

Understanding the damped free vibration plays a fundamental role in time history analysis in the next section. When the seismic analysis is performed, the system no longer makes free vibrations, and the solution of the system is divided into two categories: homogeneous and particular. A homogeneous solution is damped free vibration. A homogeneous solution is a damped free vibration of the system (transient response).

6.3 Forced Vibration

Forced vibration is excited by an external force, unlike free vibration. The dynamic analysis part of the study formulates these forces as harmonic forces (sinusoidal). Forced vibration is a two-component solution. These are the homogeneous solution and particular solution. Equation 6.8 represents the homogeneous solution (transient) in damped free vibration, while the details of the particular solution (steady-state) follow below.

$$u(t) = u_h(t) + u_p(t) \tag{6.11}$$

$$u_p(t) = C \sin(\omega t) + D \cos(\omega t) \tag{6.12}$$

Where the coefficients are:

$$C = \frac{P_0}{k} \frac{1 - (\omega/\omega_n)^2}{[1 - (\omega/\omega_n)^2]^2 + [2\zeta(\omega/\omega_n)]^2} \tag{6.13}$$

$$D = \frac{P_0}{k} \frac{-2\zeta(\omega/\omega_n)}{[1 - (\omega/\omega_n)^2]^2 + [2\zeta(\omega/\omega_n)]^2} \tag{6.14}$$

Using these coefficients, the system's amplitude reaches very high values when the force acting on it and its natural frequency are equal or close. When looking at the coefficient D, if the damping ratio is minimal, the amplitude (displacement) reaches giant values. Within this context, resonance can be prevented by either increasing the damping or altering the natural frequency of the system.

In forced vibration, only a specific harmonic force is valid and can be formulated, whereas in time history analysis, any time-defined force function can be solved, and numerical methods are based.

6.4 Modal Analysis of Existing Bridge

With modal analysis, the natural frequencies and mode shapes of the bridge system in different modes were obtained. Undamped free vibration is used as the basis.

$$\mathbf{M}\,\ddot{\mathbf{u}} + \mathbf{K}\,\mathbf{u} = \mathbf{0} \tag{6.15}$$

Where M is the mass matrix and K is the stiffness matrix.

In the study, the basis of modal analysis, finding natural frequencies and understanding mode shapes are explained with a two-degree-of-freedom system. First, the displacement vector for the 2DOF system is written as simple harmonic motion.

$$\begin{Bmatrix} u_1(t) \\ u_2(t) \end{Bmatrix} = \begin{bmatrix} a_1 \\ a_2 \end{bmatrix} \cos(\omega t - \phi) \tag{6.16}$$

Where a_1 and a_2 are the amplitudes, and ϕ is the phase angle.

The displacement vector in Equation 6.16 is derivatised twice and converted to an acceleration vector and written by substituting the values in Equation 6.15 and dividing by $\cos(\omega t - \phi)$. The final expanded form is as follows:

$$\begin{bmatrix} (k_1 + k_2) - \omega^2 m_1 & -k_2 \\ -k_2 & (k_2 + k_3) - \omega^2 m_2 \end{bmatrix} \begin{bmatrix} a_1 \\ a_2 \end{bmatrix} = \begin{bmatrix} 0 \\ 0 \end{bmatrix} \tag{6.17}$$

This is the eigenvalue problem for your 2DOF system, and to solve it, the determinant of the coefficient matrix is set equal to zero and solved for ω. The result is the natural frequencies of the system. The value a_1/a_2 gives the amplitude ratio and is used to obtain the natural mode shape. In this context, matrix multiplication is performed for Equation 6.17, and the amplitude ratio is shown for the 2DOF system.

$$\frac{a_1}{a_2} = \frac{k_2}{(k_1 + k_2) - \omega^2 m_1} \tag{6.18}$$

To illustrate with a simple example, assume an amplitude ratio of $a_1/a_2 = +0.5$ for the first natural frequency solution and $a_1/a_2 = -1.5$ for the second natural frequency solution.

$$\begin{Bmatrix} u_1(t) \\ u_2(t) \end{Bmatrix} = \begin{bmatrix} 0.5 \\ 1 \end{bmatrix} \cos(\omega_1 t - \phi_1) + \begin{bmatrix} -1.5 \\ 1 \end{bmatrix} \cos(\omega_2 t - \phi_2) \tag{6.19}$$

Figure 6.3: *Example Mode Shape for 2DOF*

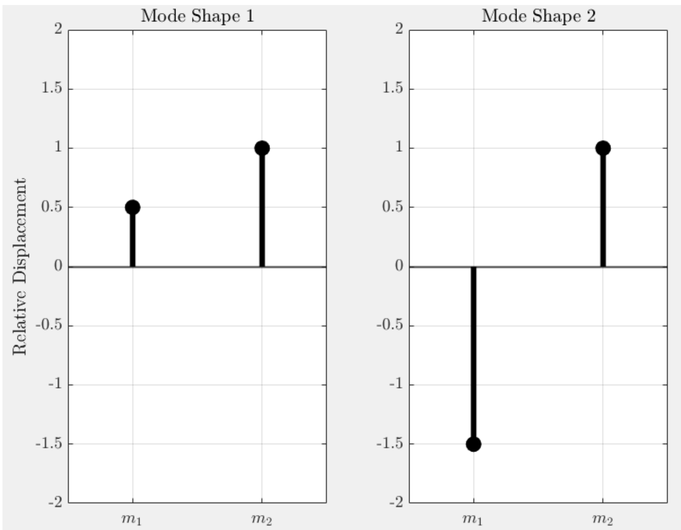

Since the degree of freedom of the studied bridge is very high, modal analysis was performed with the finite element software SAP2000. In other words, hundreds of modes may be present in large systems. However, not all of these modes are critical for the response of the structure. As a result of the modal analysis, comments can be made about the dominant modes by focusing on the mass participation ratio, which shows the rate at which the total mass in the structure moves together.

Table 6.1: *Modal load participation ratios*

OutputCase	ItemType	Item	Static (%)	Dynamic (%)
MODAL	Acceleration	UX	99.9569	96.259
MODAL	Acceleration	UY	99.9595	91.6601
MODAL	Acceleration	UZ	98.7255	58.5947

When the mass contributions to the modes are analysed, the first mode $UY = 43.16\%$, i.e., transverse motion, will be observed. When the third mode is analysed$UX = 64.74\%$, i.e., longitudinal motion is dominant. In the fifth mode, it is subjected to torsion in the plane with $RZ = 31.55\%$, respectively. This is the first impression, thanks to the tables given by SAP2000. The natural frequencies and mode shapes (motions) of six modes analysed in the study are shown in the bottom tables and figures.

Table 6.2: *Mode numbers and frequencies*

Mode Number	Frequency (Cyc/sec)
1	3.9766
2	4.0519
3	4.5828
4	4.6073
5	6.2010
6	6.7337

Figure 6.4: *First Mode – Transverse + Vertical*

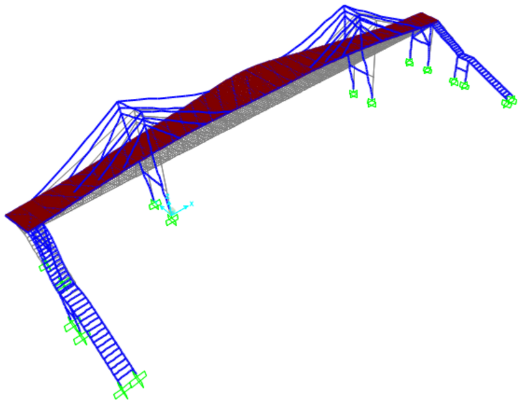

Figure 6.5: *Second Mode – Vertical*

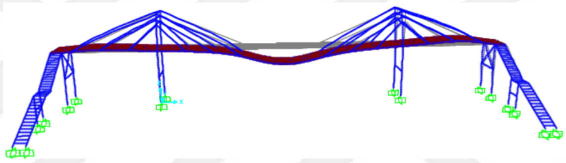

Figure 6.6: *Third Mode — Longitudinal*

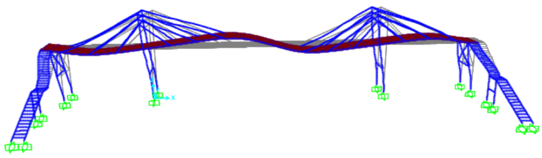

Figure 6.7: *Fourth Mode — Torsion*

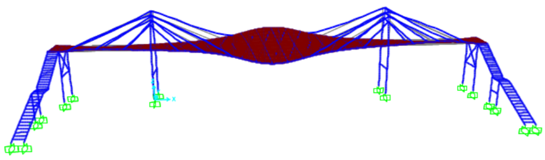

Figure 6.8: *Fifth Mode — Torsion*

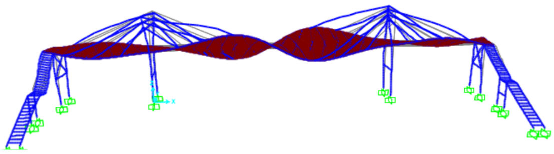

Figure 6.9: *Sixth Mode – Vertical*

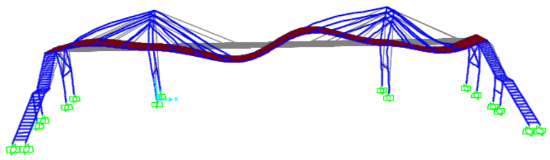

6.5 Dynamic Analysis: Linear Time History

In order to evaluate the dynamic performance of the existing bridge more realistically, a linear time history analysis was performed using ground acceleration data from previous earthquakes. The earthquake records used here represent external excitation such as dynamic wind load, pedestrian traffic, vehicle vibrations passing under the bridge, and vibrations from machinery operating around the bridge, which affect the structure and cannot be determined precisely and will be discussed in the operational modal analysis section in the next chapter. The objective is to excite the bridge in all three axes. For this reason, the earthquake records used have been scaled, and filtering has been applied in the MATLAB [32] code to focus on the three fundamental modes in the results.

The earthquake ground acceleration record used in the time history is from the Imperial Valley (El Centro) earthquake on June 6, 1940. Data in the x, y and z directions were obtained from the PEER NGA Strong Motion Database [33]. This data is defined as a function in SAP2000 in the load case section.

Figure 6.10: *Acceleration–Time History of Imperial Valley (El Centro) Earthquake—B-ELC000 Horizontal (x-axis) component*

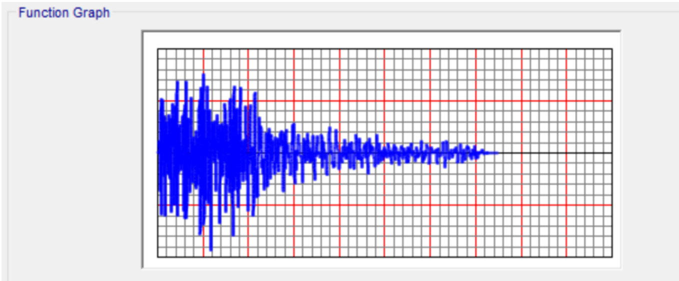

Figure 6.11: *Acceleration–Time History of Imperial Valley (El Centro) Earthquake—B-ELC0090 Horizontal (y-axis) component*

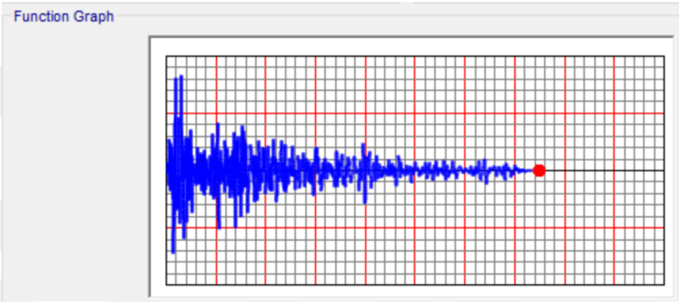

In the time history analysis, the external force identified directly affects the structure over time, and the structure's response at each time step is calculated. This allows the system's time-dependent response to be observed in detail. As a result of time history analysis conducted on the bridge, a total of 5 nodes were selected in the main span of the bridge deck, and acceleration-time graphs for these nodes were obtained. These 5 nodes represent the locations where accelerometers are planned to be installed for operational modal analysis. The data obtained from the nodes were subjected to a Fast Fourier Transform and converted to the frequency domain.

Figure 6.12: *Selected Nodes on the deck*

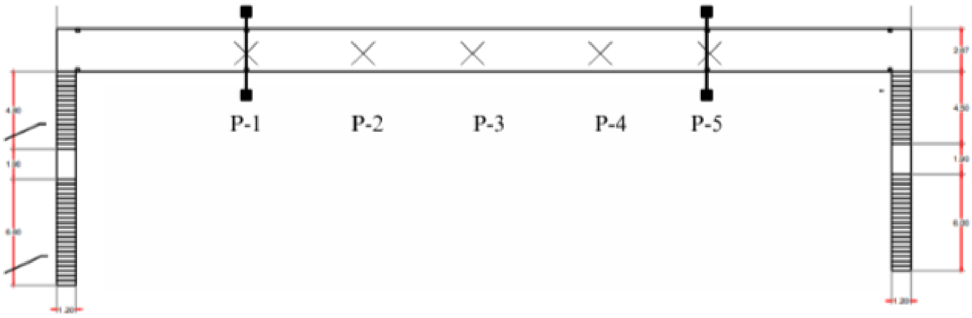

Figure 6.13: *ACC-Time Graphs and FFT Graphs for P-1: (a) X direction (b) Y direction (c) Z direction*

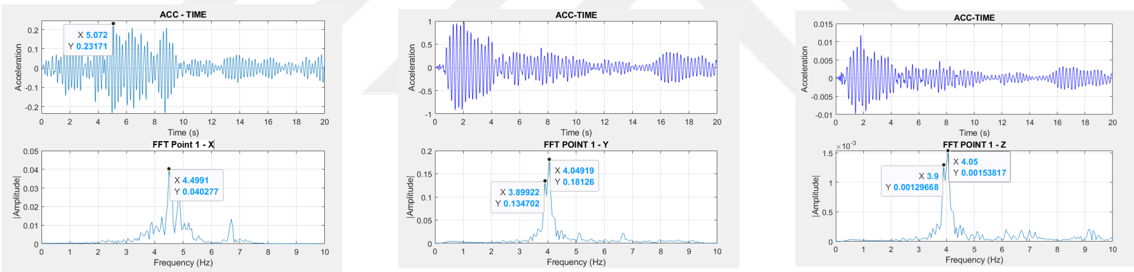

(a) *(b)* *(c)*

Figure 6.14: *ACC-Time Graphs and FFT Graphs for P-2: (a) X direction (b) Y direction (c) Z direction*

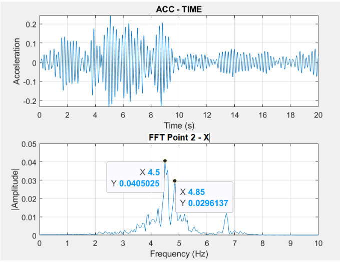

(a)

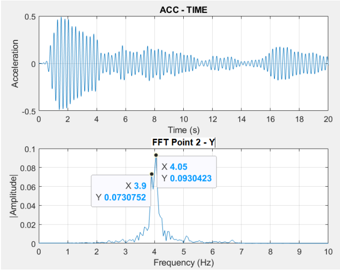

(b)

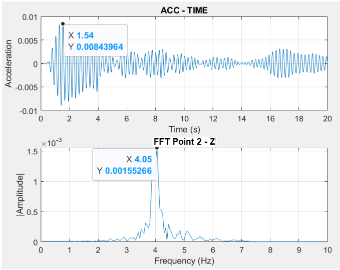

(c)

Figure 6.15: *ACC-Time Graphs and FFT Graphs for P-3: (a) X direction (b) Y direction (c) Z direction*

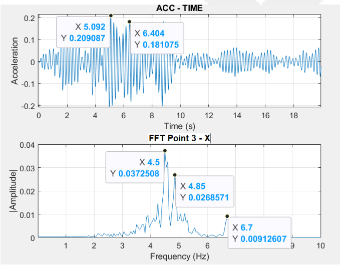

(a)

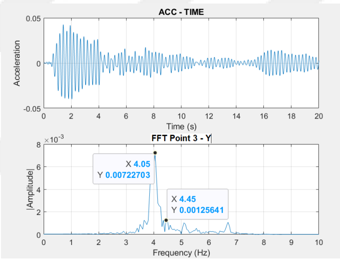

(b)

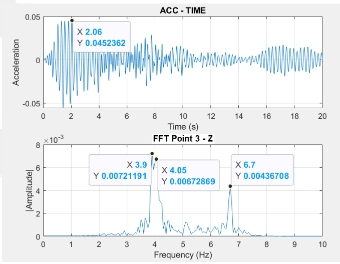

(c)

Figure 6.16: *ACC-Time Graphs and FFT Graphs for P-4: (a) X direction (b) Y direction (c) Z direction*

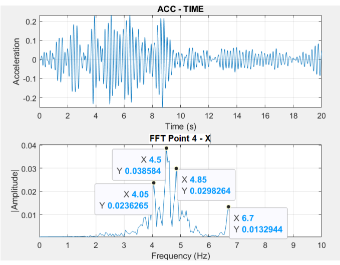

(a)

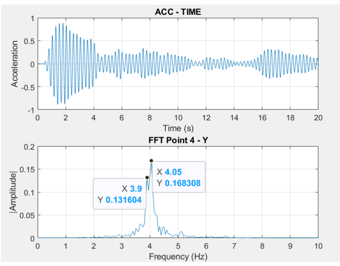

(b)

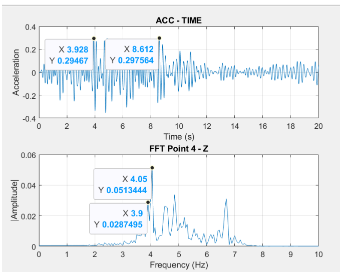

(c)

Figure 6.17: *ACC-Time Graphs and FFT Graphs for P-5: (a) X direction (b) Y direction (c) Z direction*

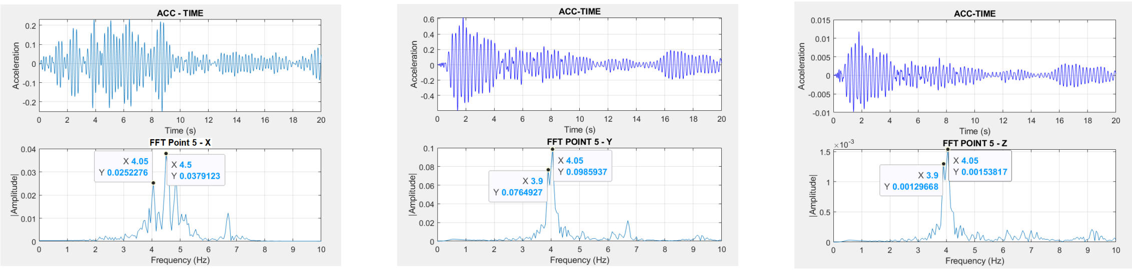

(a) *(b)* *(c)*

The modal analysis results can be checked using FFT graphs obtained from time history analysis. It should be noted that when an external force or external excitations is applied to a structure, the structure's response peaks at its natural frequencies or values close to its natural frequencies. This phenomenon represents resonance. Therefore, understanding the dynamic characteristics of a structure is important for determining the structure's response and for resonance control.

7. EXPERIMENTAL STUDIES

Natural frequencies and mode shapes were derived in the study's analytical section. Operational Modal Analysis (OMA) was performed on the bridge to evaluate the accuracy of these results. In the finite element model, there will be differences between the model and the actual data due to the lack of supports, non-structural elements, nonlinear geometry, and material properties being defined with certain assumptions, and these discrepancies will be updated within the scope of the results obtained from OMA.

In the field study, operational modal analysis was performed for ambient factors such as the number of people passing through the bridge, wind, and vehicle traffic, and the dynamic properties of the system were identified based only on the output data.

Within the scope of the study, two different accelerometers were used. In the first stage, the background of the study was prepared with various measurements with Sensebox 7003-D, and the basic concepts were understood, and in the second stage, the operational model analysis and acceleration-time data were collected with SARA Ace-Boxes, and the natural frequencies and fundamental mode shapes of the structure were obtained.

7.1 Accelerometers

7.1.1 Sensebox 7003-D

The SenseBox 7003-D [34], owned and actively used since the first day of the thesis, is a high-precision digital accelerometer and tiltmeter. This device is actively used in engineering applications such as structural monitoring and vibration analysis. It is a 3-axis device in terms of technical specifications and can collect data in x, y, and z directions. The device has two outputs in total: power output and Ethernet output. It is directly connected to the computer via Ethernet and works with the monster software to which it is connected.

Figure 7.1: *Field installation SenseBox 7003-D*

Table 7.1: *Features of SenseBox 7003-D*

Category	**Specification**
Model	SenseBox 7003-D
Operating Modes	Accelerometer Mode, Tiltmeter Mode (Software Selectable)
Accelerometer Axes	3 Axes (X, Y, Z)
Tiltmeter Axes	2 Axes (X, Y)
Measurement Range (g)	± 2 / ± 4 / ± 8 g (Software Selectable)
Sampling Frequencies	125 / 250 / 500 / 1000 Hz (Software Selectable)
Resolution (g)	0.00023 g
Accuracy (g)	0.001 g
Noise Level	30 $\mu g/\sqrt{\mathrm{Hz}}$ (in ± 2 g range)

Monster software was installed on the computer by TDG company [34]. In the first stage, the device and sensors were defined in the editor section, and in the second stage, recording operations were performed. Three sensors were set to record the acceleration-time data of the position of the device in x, y and z directions. While the software records displacement-time data, FFT results are not included. In order to switch to the frequency domain, FFT is applied to the recorded values via MATLAB [32].

With its easy portability and low-cost structure, SenseBox has provided an accessible solution, especially for student projects and academic research. In this context, a large amount of acceleration-time data was collected through the device and played a fundamental role in understanding the dynamic behaviour of the structure. The results of the first field study carried out during the project revealed that the device is particularly sensitive to environmental noise, which causes certain deviations in the measurement results. Accordingly, additional filtering was needed in order to reach more reliable results in data analysis.

7.1.2 SARA AceBox

SARA AceBox [35], the measurement device used in the operational modal analysis part of the study, is a high-precision digital acceleration recorder developed for strong ground motion monitoring and structural health monitoring. With its advanced sensor structure and integrated data logger unit, it is actively used in field measurements.

As can be seen in Figure 7.2, both the accelerometer sensor and the data logger unit are integrated in the main red box and record structural vibrations. The other large red box is the portable power supply used to ensure long-term and uninterrupted operation of the device in the field environment. The black box is the GPS module for time synchronisation. Measurement data can be exported via USB or Ethernet cable.

With 5 accelerometers included in the operational analysis part of the study, data were collected at different points on the bridge deck and played an important role in reaching the natural frequencies and fundamental mode shapes of the structure.

Figure 7.2: *Field installation SARA AceBox*

Table 7.2: *Features of SARA AceBox*

Category	**Specification**
Model	SARA AceBox
Operating Modes	Strong Motion Monitoring, Structural Health Monitoring
Accelerometer Type	Force Balance Accelerometer (Electrodynamic)
Accelerometer Axes	3 Axes (X, Y, Z)
Measurement Range (g)	± 0.5 / ± 1 / ± 2 / ± 4 g (Selectable)
Sampling Frequencies	1 – 1500 Hz (Selectable)
Resolution	238 nano-g/count (at ± 2 g)
Noise Level	$< 20\,\mathrm{ng}/\sqrt{\mathrm{Hz}}$
Dynamic Range	> 165 dB (Sensor), > 140 dB (System)
Time Sync Method	GPS or NTP
Internal Memory	From 16 GB up to 8 TB
Data Formats	GSE, SAC, SAF, miniSEED, SEG2, etc.
Communication	USB, Ethernet, RS232

7.2 Operational Modal Analysis

Operational Modal Analysis is a methodological approach used to identify the dynamic characteristics of structures operating under ambient influences, applied solely using output data without considering input data. This method analyses the responses of a structure under environmental influences such as wind force, pedestrian traffic, vehicle passage, and active machinery, using only the structure's output data. This approach was first used in Japan by Omori in the field of earthquake engineering [36, 37]. In recent years, studies on determining the dynamic characteristics of using OMA have increased, and different techniques offer different analysis approaches [16, 38]. In the thesis field study, the simple method of frequency domain methods and Peak Picking (PP) were chosen for the identification of dynamic characteristics due to their ease of application [39, 40]. This technique is based on Fast Fourier Transform (FFT) and determines the natural frequency through the peak points in the Power Spectrum Density (PSD), how much vibration energy the structure receives at which frequency, and curves obtained from the vibration records of the structure.

Field data was recorded on 23.04.2025. Measurements were recorded using SARA Acebox force-balanced accelerometers [35] capable of recording in three axes, with 20-minute recording intervals, to measure acceleration-time data on the bridge deck. The five accelerometers on-site were positioned at five nodes, shown in Figure 6.12, selected based on time history analysis performed in the analytical model.

Figure 7.3: *Field installation of the SARA AceBox at different locations: (a) left view, (b) right view*

(a) *(b)*

MATLAB [32] was used for the frequency domain analysis of the acceleration data obtained from the X, Y and Z directions, and a conversion to the frequency domain was performed. In the MATLAB code executed, the frequency range was set to 0-10 Hz in order to clearly see only the fundamental modes.

The ambient vibration survey was conducted to measure the vibrations to which the structure is naturally exposed. The dynamic responses of the bridge were measured under low-amplitude vibrations caused by external excitation such as wind forces, pedestrian traffic, vibrations generated by vehicles passing under the bridge, and vibrations generated by machinery used near the existing bridge. The figures below show the acceleration data collected from the field and the frequency graphs converted from this data.

Figure 7.4: *Collected Data X - Longitudinal*

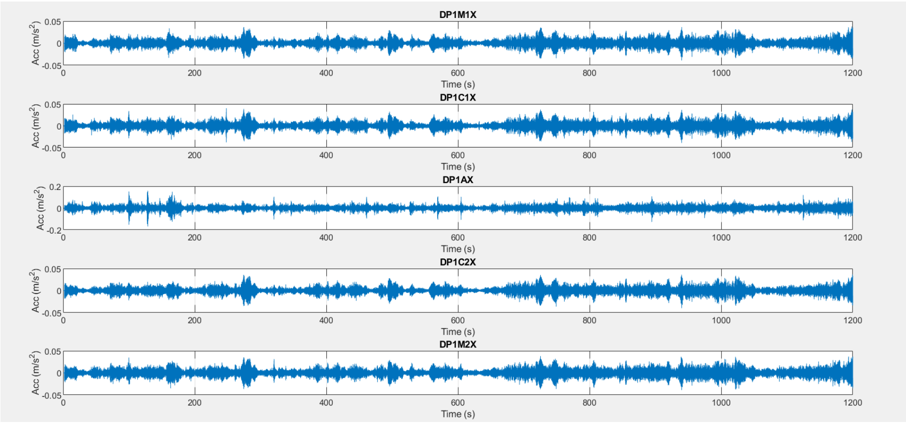

Figure 7.5: *Collected Data Y - Transverse*

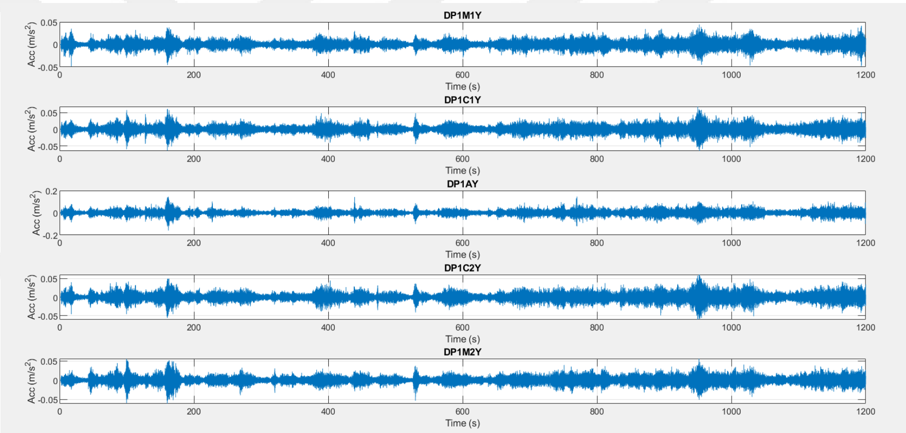

Figure 7.6: *Collected Data Z – Vertical*

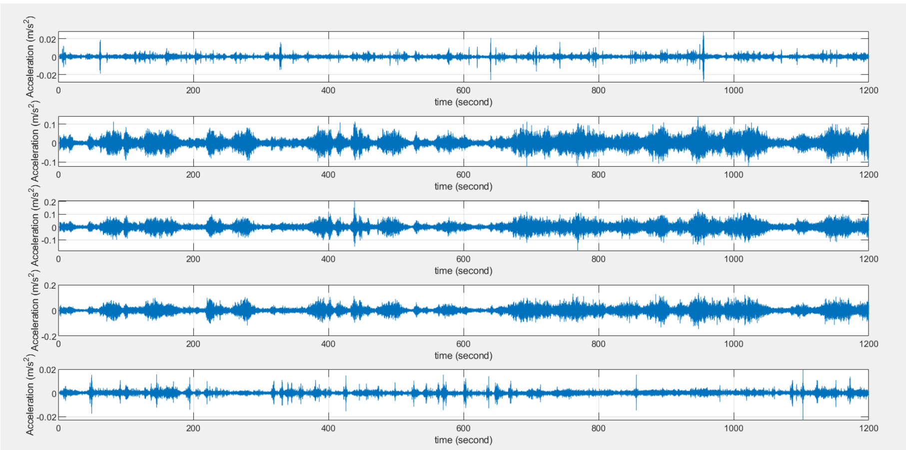

Figure 7.7: *Operational Modal Analysis results*

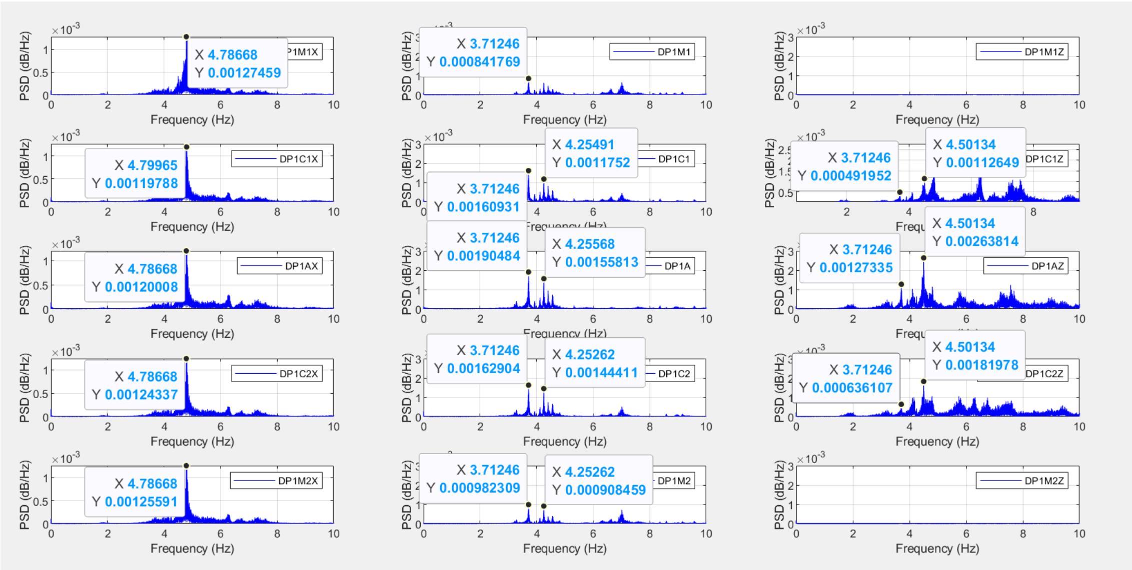

When the experimental results are examined, the graphs in the first column represent the x-axis, the graph in the second column represents the y-axis, and the FFT graphs in the last column represent the z-axis. The top graph represents point 1, shown in Figure6.12 while the bottom graph represents point 5.

The natural frequency obtained from the five points on the axis, 4.79, clearly represents the longitudinal movement. From this point, the first priority in the model calibration section is to capture the movement on the x-axis.

When the measurements on the y-axis are examined on a frequency basis, two different peak values are observed. The first is 3.71, and the second is 4.25. It is not possible to make a clear interpretation here because common movement is observed on the y and z axes in the mode shapes obtained in the analytical model. For this reason, a clearer interpretation can be made after examining the z-axis.

When the results of the accelerometers on the z-axis are examined, the results of the accelerometers located in the pylon regions are not effective because their amplitude values are very small. This is expected because the axial rigidity is very high. When the three accelerometers in the middle are examined, clear pickers are observed at 3.71 and 4.50.

When the Y and Z graphs are examined together, the 3.71 Hz movement in both graphs represents a common movement. It has been determined that the first mode is 3.71 and that there is common movement in the mode shape. For the second mode, it is thought that the value will be between 4.25 and 4.50 and that there may be common mass participation in the mode shape. The longitudinal mode is 4.79 Hz

8. COMPARISON OF RESULTS, MODAL UPDATING AND DISCUSSION

8.1 Comparison

First, analytical natural frequencies and mode shapes were obtained from a three-dimensional finite element model created using the dimensions of cross-sections and structural elements obtained in detail during field research. Then, experimental results were obtained through operational model analysis in the field. When the results were compared, there was an error rate, although it was not high. Thanks to the accelerometers placed at different points on the field, the mode shape is clearly understood and is consistent with the mode shapes obtained in the analytical model.

Table 8.1: *Analytical vs. Experimental Frequencies with error rates*

Mode	Analytical (Hz)	Experimental (Hz)	Error (%)
First	3.97	3.71	7.01
Second	4.05	4.50	10.00
Third	4.58	4.79	4.38

The main reasons for the differences:

- Material properties such as elasticity modulus (E), structural geometry, and damping ratio are accepted as standard in the software program. However, differences may arise during the construction process or production process. In other words, differences between design and application.
- Factors that may affect system rigidity, such as corrosion, damage, connection loosening, and fatigue that may occur over time in the actual structure, are ignored.
- Unless specifically stated during modelling, connections are defined as fully rigid connections. Therefore, they cannot fully represent the actual behaviour.

- Elements such as asphalt and railings are integrated into the model as additional mass, but their contribution to rigidity is not taken into account.
- The end supports under the foundation are defined as fixed. However, the behaviour of the existing structure is not fully represented.
- Details such as stiffeners present in the structure are not available in the software program, but their effects should be considered.

8.2 Modal Updating

The numerical models developed may not always accurately reflect the actual behaviour due to the uncertain parameters provided in the comparison section. Modal parameters such as natural frequencies, mode shapes, and sometimes the damping ratio, measured through modal updating, are used to update the numerical model. H. Tran et al. [41] emphasised that a few modes with high participation factors are sufficient for obtaining the dynamic characteristics. In the cable-stayed steel pedestrian bridge study, the focus was on the first three modes with high mass participation.

There are different approaches in the literature for model calibration. However, the process is primarily based on two main parameters: mass and stiffness. Özçelik et al. [42] conducted their study on the end supports of columns. They applied 10 kN loads in three directions to the columns and determined the stiffness values from the load/displacement relationship in three axes. Initially, an analytical model was created using pin connections, and in the model update phase, comparisons were made with the spring model frequencies. The natural frequency values obtained in the spring system also showed an increase of 10% to 15% In the update section of their study.

Petersen et al. [43]changed the elastic modulus of structural elements by 3% to 5% while changing the density values by 5% to 15%. It is noteworthy that while all elements were reduced, only the elastic modulus of the girder was increased. Similarly, Bayraktar et al. [39] reduced the modulus of elasticity and densities in the calibration section.

Tran et al. [41] measured the vibration of an existing truss system in the field and created an analytical model. The main focus of their work was the stiffness conditions of the joints. In the first stage, they used pin connections, in the second stage rigid connections, and in the final stage semi-rigid connections. When they analysed the three different connection types using field data, they found that the semi-rigid connection closely matched the actual behaviour. There was approximately a 25% difference between the semi-rigid and rigid connections and approximately a 15% difference between the pin and semi-rigid connections.

The analytical model of the cable-stayed pedestrian bridge under investigation was created after numerous visits to the site with the aim of developing a detailed model. The error rate was found to be low, indicating that the model accurately represents the actual structure. However, in line with the studies in the literature, the density of the material properties of the structural elements in the model was reduced by 5%.

Figure 8.1: *Material properties*

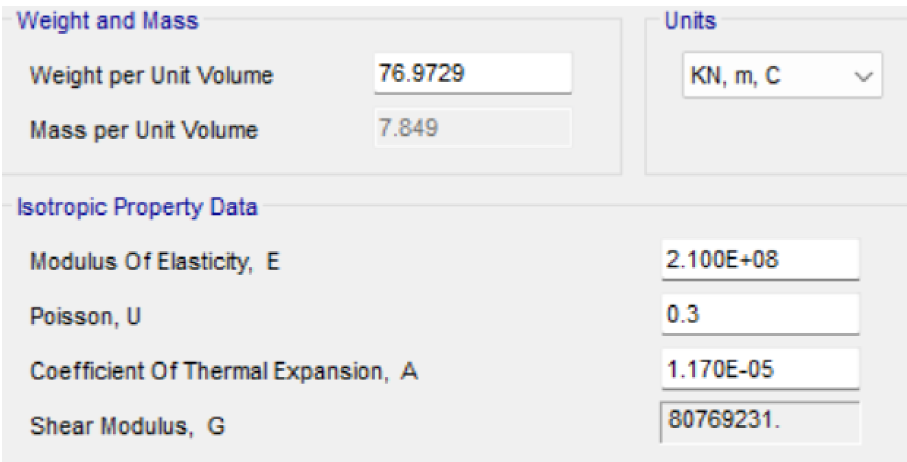

When analytical frequencies are compared with experimental frequencies, it is observed that the transverse mode is higher in the analytical model. In this context, the

Table 8.2: *Updated weight per Unit Volume after 5% reduction*

Property	**Updated Value**
Weight per Unit Volume (kN/m^3)	73.124
Mass per Unit Volume (t/m^3)	7.4566

stiffness of the pylons and columns effective in transverse motion was reduced by 25% in the weak axis. Unlike the studies reviewed in the literature, a property modifier was preferred in this reduction process. Since the objective was to intervene in the bending stiffness of the columns along their weak axis, the bending moment in the weak direction was multiplied by a coefficient, and the analysis was continued directly through the bending stiffness.

Figure 8.2: *Stiffness update in the vertical elements*

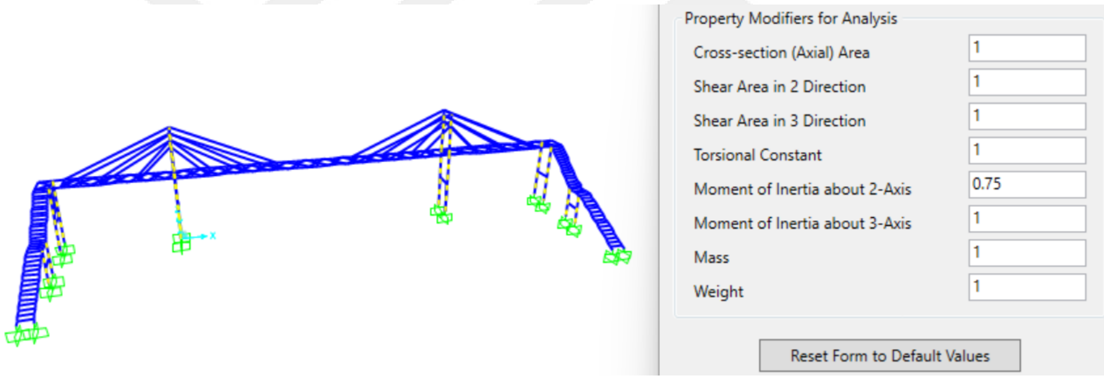

Similarly, when considering the deck system, many elements are connected to the web section of the edge beams. While these connections are assumed to be completely rigid in the finite element model, the bending rigidity in the weak axis has been reduced by 25%. However, since the structure of the deck system has not been fully modelled, the stiffness of the additional elements has been defined as an additional 20% in the strong axis of the edge beam.

Figure 8.3: *Stiffness update in the Deck system*

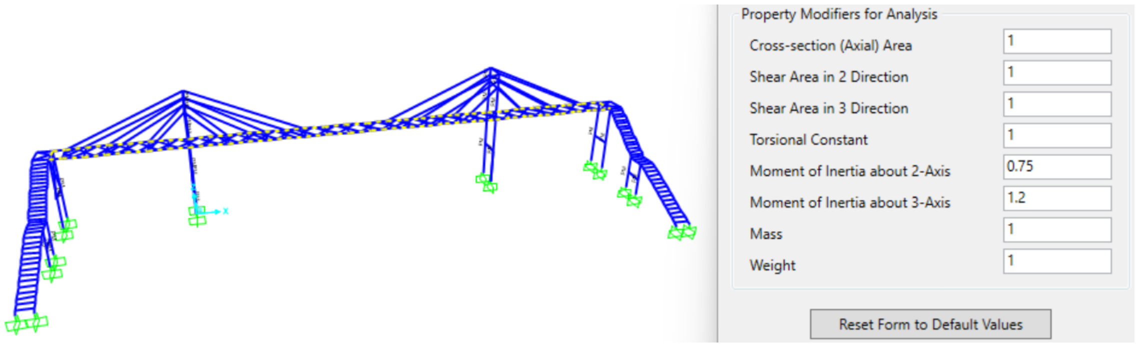

8.3 Discussion

First, the mass was reduced on the model, resulting in increased frequencies. Considering the design, production, and field application of structural elements and reviewing the literature, a 5% reduction is appropriate because it results in lower values than the analytical model's field data in both the vertical and longitudinal modes.

When examining the first mode shape, which is the vertical and transverse common motion, it was determined that the dominant motion is the weak axis of the vertical elements, and accordingly, the EI value was reduced. While reducing the EI value, the reduction was not made directly through the elastic section modulus as in the studies in the literature. Considering the connection conditions, the EI value was multiplied by a coefficient to reduce the contribution of the connection, which was completely rigid in the analytical model, to the system. Thus, when the connection conditions changed, the effective rigidity of the system also changed. A definitive comment cannot be made about the type of connection formed by the transverse beams and bracings connected to the web (weak axis) of the edge beams. Similarly, the EI value was multiplied by a low coefficient to reduce the effective rigidity. However, since the deck system in the model does not fully reflect the system in the actual bridge, the rigidity of the elements directly taken as dead load in the model was added to the beam's strong axis.

Table 8.3: *Comparison of Experimental and Analytical Frequencies before and after Model Updating*

Mode	Direction	Experimental (Hz)	Analytical Before (Hz)	Error (%)	Analytical After (Hz)	Error (%)
1	Transverse + Vertical (Y + Z)	3.71	3.97	7.01	3.82	2.97
2	Vertical (Z)	4.50	4.05	10.00	4.16	7.56
3	Longitudinal (X)	4.79	4.58	4.38	4.69	2.09

When examining the table generated with the updated analytical values, a significant decrease in the error rate of the 1st and 3rd modes is observed, and a result close to the actual behaviour has been obtained. However, when examining the 2nd vertical mode, it is observed that the effects of the aforementioned processes are not as effective as those on the other modes. Looking back at the operational model analysis, the first peak value in the FFT graphs obtained on the y-axis was 3.71, and the second peak value was 4.25. When examining the z-axis, the first peak value was again 3.71, and the other peak value was 4.50. Based on this, when returning to the analytical model and examining mass participation, it was noted that participation in the first mode was 62%, while participation in the second mode was 14%. In conclusion, it is assessed that this mode does not belong to a specific axis and that its frequency value can be defined within the range of 4.25 to 4.50 Hz.

Figure 8.4: *Mode Shapes: (a) First Mode (b) Second Mode (c) Third Mode*

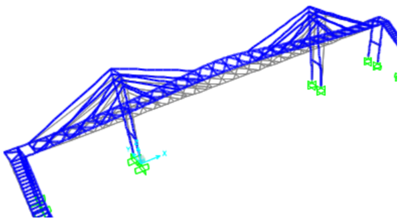

(a)

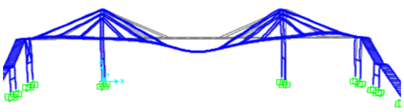

(b)

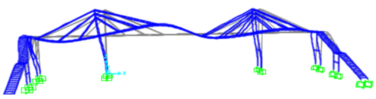

(c)

9. CONCLUSIONS

In this thesis study, the dynamic behaviour of the Taşdelen pedestrian cable-stayed bridge located in Istanbul has been investigated in detail using both analytical and experimental methods. Within the scope of the study, the geometry of the bridge, the dimensions of the load-bearing elements and their section properties were determined through field investigations, and a finite element model was developed and detailed in the numerical study. Vertical and horizontal structural elements, cables, bracings, slabs, and their properties are detailed in Section 3. In the numerical study section, various codes were used to apply vertical and wind loads to the model, and the static analysis of the existing bridge was performed. The results of the static analysis showed that the capacity is significantly higher than the applied load.

Following the modelling studies, the mathematical foundation for vibration analysis was established to determine the dynamic characteristics of the existing bridge. From this foundation, modal analysis was first carried out to obtain the fundamental mode shapes and natural frequencies of the bridge. Within the scope of dynamic analysis, a linear time history analysis was performed on the model. Here, previously recorded earthquake ground motion data was scaled and defined in the SAP2000 software, followed by the analysis. One of the significant advantages of time history analysis is that it shows the responses of the nodes in the structural elements at every time step. For this reason, time history analysis was preferred in many dynamic analyses, and as a result, acceleration-time graphs were obtained for five nodes selected on the deck. By applying FFT to the obtained data, the frequency domain was accessed, and resonance effects were specifically demonstrated by observing distinct peaks at points corresponding to or near the natural frequency.

In the experimental studies, acceleration data were collected in three axes (X, Y, and Z) using accelerometers installed at the five node points previously selected in the time history on the bridge structure. In the operational modal analysis, low-amplitude environmental excitation such as wind, human traffic, and vibrations caused by vehicles passing under the bridge were effective, and the frequency components were obtained by applying FFT to the output data.

As a result of comparing the analytical and experimental findings, it was determined that the model showed deviations from the experimental data in some mode shapes. The main reasons for these deviations were identified as the connections in the analytical model, material parameters, and element stiffness not fully matching the real system. In particular, the accuracy of stiffness and mass parameters is known to play a critical role in determining natural frequencies, and model update studies were carried out in this context. In the update section, the literature was reviewed, and changes were made to parameters such as pylon stiffness, deck system stiffness, and density to improve the agreement between the model results and experimental data and minimise the error rate.

During the model update process, the mass of the analytical model was first reduced by 5%, which resulted in an increase in the frequency value of the analytical model. Considering similar studies in the literature and the manufacturing and field applications of the bridge, this level of mass reduction was implemented. However, instead of directly reducing the bending stiffness (EI) to reduce the rigidity of the weak axis, the effective stiffness was reduced by multiplying it by coefficients representing the contribution of the connection conditions to the system. The same approach was applied to the deck system, but the total effective stiffness of the system was increased in the strong direction by considering the stiffness of elements not present in the model. When the updated analytical frequencies were compared with the experimental frequencies, a significant decrease in the error rates was observed, particularly in the first and third modes. However, the relatively high error rate in the vertical mode is due to the fact that this mode has a complex mode character rather than being specific to a particular axis.

In conclusion, this study has comprehensively evaluated the dynamic behaviour of the Taşdelen pedestrian bridge using both an analytical model and experimental measurements. Through modal analysis, time history, FFT evaluations, and model updates, the natural frequencies, mode shapes, and parameters influencing these dynamic characteristics of the bridge have been systematically analysed. The results obtained are guiding for vibration analyses and model validation studies to be conducted on similar structures. Additionally, the increased accuracy of the analytical model calibrated with field data provides a robust foundation for future seismic analyses or long-term monitoring studies.

REFERENCES

[1] CSI America, "Sap2000 - user interface features," n.d. Retrieved from `https://www.csiamerica.com/products/sap2000/features/user-interface`.

[2] Eurocode Applied, "Ipe, hea, heb, hem design properties," n.d. Retrieved from `https://eurocodeapplied.com/design/en1993/ipe-hea-heb-hem-design-properties`.

[3] AASHTO, *LRFD Bridge Design Specifications*. American Association of State Highway and Transportation Officials, 9th ed., 2020.

[4] CEN (European Committee for Standardization), *EN 1993-1-1: Eurocode 3: Design of steel structures – Part 1-1: General rules and rules for buildings*. Brussels, Belgium: CEN, 2005.

[5] Türkiye Standartları Enstitüsü, *TS EN 1991-1-4: Yapılar Üzerindeki Etkiler – Bölüm 1-4: Genel Etkiler – Rüzgâr Etkileri*. TSE Yayınları, 2005.

[6] A. K. Chopra, *Dynamics of Structures: Theory and Applications to Earthquake Engineering*. Pearson, 5 ed., 2017.

[7] W. T. Segui, *LRFD Steel Design*. CL Engineering, 2003.

[8] R. Jayaraman, B. Sellamuthu, and T. N. Ponnu Durai, "Design of cable stayed pedestrian bridge," *International Journal of Applied Engineering Research*, vol. 10, no. 53, pp. 24–32, 2015.

[9] C. Alocci and P. S. Valvo, "Feasibility study of a hybrid frp-steel cable-stayed pedestrian swing bridge," *Engineering Structures*, vol. 189, pp. 359–372, 2019.

[10] B. Atmaca, "Size and post-tensioning cable force optimization of cable-stayed footbridge," *Structures*, vol. 33, pp. 2036–2049, 2021.

[11] G. Polepally, V. D. K. Pasupuleti, and A. Dongre, "Comparison of different types of pylon shapes on seismic behavior of cable-stayed bridges," in *Lecture Notes in Civil Engineering*, pp. 69–80, 2020.

[12] J. Cheng and F. Dong, "A simplified method for free vibration analysis of cable-stayed bridges," *International Journal of Steel Structures*, vol. 16, no. 1, pp. 151–162, 2016.

[13] F. Aras, "Effects of ambient temperature and magnitude of the vibration on the dynamics of pre-stressed precast isolated pedestrian bridges," *Turkish Journal of Civil Engineering*, vol. 35, no. 1, pp. 23–40, 2023.

[14] L. Zhang, G. Qiu, and Z. Chen, "Structural health monitoring methods of cables in cable-stayed bridge: A review," *Measurement*, vol. 168, p. 108343, 2021.

[15] F. Aras, "Modal testing of an isolated overpass bridge in its construction stages," *The Baltic Journal of Road and Bridge Engineering*, vol. 13, no. 1, pp. 67–76, 2018.

[16] F. Magalhaes, E. Caetano, and A. Cunha, "Challenges in the application of stochastic modal identification methods to a cable-stayed bridge," *Journal of Bridge Engineering*, vol. 12, no. 6, pp. 746–754, 2007.

[17] F. Tubino, L. Carassale, and G. Piccardo, "Human-induced vibrations on two lively footbridges in milan," *Journal of Bridge Engineering*, vol. 21, no. 8, 2016.

[18] F. Au, Y. Cheng, Y. Cheung, and D. Zheng, "On the determination of natural frequencies and mode shapes of cable-stayed bridges," *Applied Mathematical Modelling*, vol. 25, no. 12, pp. 1099–1115, 2001.

[19] W. Ren, X. Peng, and Y. Lin, "Experimental and analytical studies on dynamic characteristics of a large span cable-stayed bridge," *Engineering Structures*, vol. 27, no. 4, pp. 535–548, 2005.

[20] J. A. Gonilha, J. R. Correia, F. A. Branco, E. Caetano, and A. Cunha, "Modal identification of a gfrp-concrete hybrid footbridge prototype: Experimental tests and analytical and numerical simulations," *Composite Structures*, vol. 106, pp. 724–733, 2013.

[21] A. Gheitasi, O. E. Ozbulut, S. Usmani, M. Alipour, and D. K. Harris, "Experimental and analytical vibration serviceability assessment of an in-service footbridge," *Case Studies in Nondestructive Testing and Evaluation*, vol. 6, pp. 79–88, 2016.

[22] R. Brockenbrough and F. Merritt, *Structural Steel Designer's Handbook*. McGraw Hill Professional, 1999.

[23] AISC (American Institute of Steel Construction), "Steel bridge design handbook," n.d. Retrieved from `https://www.aisc.org/nsba/design-and-estimation-resources/steel-bridge-design-handbook/`.

[24] D. L. Logan, *A First Course in the Finite Element Method*. Thomson Learning, 2007.

[25] K. Bathe, *Finite Element Procedures*. 1995. Retrieved from `http://archives.umc.edu.dz/handle/123456789/116606`.

[26] D. Mertz and J. Dubois, *Steel Bridge Design Handbook: Chapter 7 – Loads and Load Combinations*. American Institute of Steel Construction, 2022.

[27] J. Cheng, J. Jiang, R. Xiao, and H. Xiang, “Ultimate load carrying capacity of the lu pu steel arch bridge under static wind loads,” *Computers & Structures*, vol. 81, no. 2, pp. 61–73, 2003.

[28] R. Yin, B. Zhu, S. Yuan, J. Li, Z. Yang, and Z. Yang, “Dynamic analyses of long-span cable-stayed and suspension cooperative system bridge under combined actions of wind and regular wave loads,” *Applied Ocean Research*, vol. 138, p. 103683, 2023.

[29] L. A. Zdravkov, “Wind loads on girder bridges,” *Challenge Journal of Structural Mechanics*, vol. 8, no. 1, pp. 9–16, 2022.

[30] M. Suangga and Sularno, “Comparison of wind load on standard steel truss bridge based on indonesian bridge loading codes,” *IOP Conference Series: Earth and Environmental Science*, vol. 998, no. 1, p. 012016, 2022.

[31] A. I. of Steel Construction, *Specification for Structural Steel Buildings (AISC 360-16)*. Chicago, IL: American Institute of Steel Construction, 2016.

[32] The MathWorks, Inc., “MATLAB (Version R2024a) [Computer software].” `https://www.mathworks.com/products/matlab.html`, 2024. Accessed: 2025-04-25.

[33] Pacific Earthquake Engineering Research Center (PEER), “Imperial Valley-01, El Centro Array #9, RSN 4.” `https://ngawest2.berkeley.edu`, 2014. NGA-West2 Strong Motion Database, University of California, Berkeley.

[34] T. Teknoloji, “Sensebox 7003-d - dijital İvmeölçer / tiltmetre,” 2025. Accessed: 2025-04-25.

[35] Sentez Yer ve Yapı Mühendisliği, “Sara acebox fba: Kuvvetli yer hareketi ve yapısal sağlık İzleme cihazı.” `https://syy.com.tr/sara-acebox-fba`, 2025. Erişim tarihi: 28 Mayıs 2025.

[36] C. Michel, P. Guéguen, and M. Causse, “Seismic vulnerability assessment to slight damage based on experimental modal parameters,” *Earthquake Engineering and Structural Dynamics*, vol. 41, pp. 81–98, 2012.

[37] C. Davison, “Fusakichi omori and his work on earthquakes,” *Bulletin of the Seismological Society of America*, vol. 14, no. 4, pp. 240–255, 1924.

[38] R. Brincker, L. Zhang, and P. Andersen, “Modal identification from ambient responses using frequency domain decomposition,” in *Proceedings of the 18th International Modal Analysis Conference (IMAC)*, (San Antonio, TX, USA), Society for Experimental Mechanics, February 7–10 2000.

[39] A. Bayraktar, A. C. Altunişik, B. Sevim, and T. Türker, “Modal testing, finite-element model updating, and dynamic analysis of an arch type steel footbridge,” *Journal of Performance of Constructed Facilities*, vol. 23, no. 2, pp. 81–89, 2009.

[40] F. Aras, “Frequency variation in construction stages and model validation for steel buildings,” *Steel and Composite Structures*, vol. 22, no. 3, pp. 647–662, 2016.

[41] H. Tran-Ngoc, S. Khatir, G. D. Roeck, T. Bui-Tien, L. Nguyen-Ngoc, and M. A. Wahab, “Model updating for nam o bridge using particle swarm optimization algorithm and genetic algorithm,” *Sensors*, vol. 18, no. 12, p. 4131, 2018.

[42] Özgür Özçelik, Özgür Girgin, and C. Amaddeo, “199+325 çelik demiryolu köprüsünün sistem tanımlama çalışmaları ve kalibre sonlu elemanlar modelinin oluşturulması,” *Pamukkale Üniversitesi Mühendislik Bilimleri Dergisi*, vol. 24, no. 6, pp. 1051–1061, 2018.

[43] Øyvind Wiig Petersen and O. Øiseth, “Finite element model updating of a long span suspension bridge,” in *Geotechnical*, pp. 253–260, Springer, 2019.

APPENDICES

APPENDIX A. EXISTING BRIDGE IMAGE

Figure A.1: *Tasdelen Cable-Stayed Pedestrian Bridge*

Figure A.2: *Support End Column*

Figure A.3: *Concrete Slab and Railings*

Figure A.4: *Stays Pin Connections*

APPENDIX B. LOADS AND CAPACITY CALCULATION DETAIL

Dead load calculation of concrete slab:

$$2500\,\frac{\mathrm{kg}}{\mathrm{m}^3} \times 0.08\,\mathrm{m} = 200\,\frac{\mathrm{kg}}{\mathrm{m}^2} \tag{B.1}$$

$$200\,\frac{\mathrm{kg}}{\mathrm{m}^2} \times 9.81\,\frac{\mathrm{m}}{\mathrm{s}^2} \times 10^{-3} = 1.96\,\frac{\mathrm{kN}}{\mathrm{m}^2} \tag{B.2}$$

$$1.96\,\frac{\mathrm{kN}}{\mathrm{m}^2} \times 1.9\,\mathrm{m} = 3.72\,\frac{\mathrm{kN}}{\mathrm{m}} \tag{B.3}$$

$$3.72\,\mathrm{kN/m} \div 2 = 1.86\,\mathrm{kN/m} \approx 2\,\mathrm{kN/m} \tag{B.4}$$

Live load calculation:

$$5\,\frac{\mathrm{kN}}{\mathrm{m}^2} \times 1.9\,\mathrm{m} = 9.5\,\frac{\mathrm{kN}}{\mathrm{m}} \tag{B.5}$$

$$9.5\,\mathrm{kN/m} \div 2 = 4.75\,\mathrm{kN/m} \quad \text{(each girder)} \tag{B.6}$$

Local Stability for Compression Member:

Figure B.1: *Local Stability Limitation for I-Shape [7]*

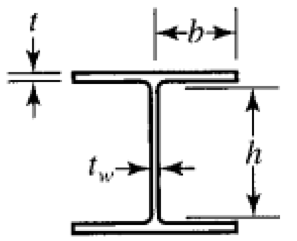

$$b/t \le 0.56\sqrt{E/F_y}$$
$$h/t_w \le 1.49\sqrt{E/F_y}$$

$$\frac{b}{t_f} = \frac{150}{32} = 4.6875 \le 0.56 \times \sqrt{\frac{210000}{235}} = 16.74 \quad \Rightarrow \quad \text{Compact} \tag{B.7}$$

$$h = D - 2 \times t_f = 700 - 2 \times 32 = 636 \text{ mm} \tag{B.8}$$

$$\frac{h}{t_w} = \frac{636}{17} = 37.41 \leq 1.49 \times \sqrt{\frac{210000}{235}} = 44.54 \quad \Rightarrow \quad \text{Compact} \tag{B.9}$$

HEB 700 values are shown in the Table 4.1

Capacity for Compression Member (Built-up Section):

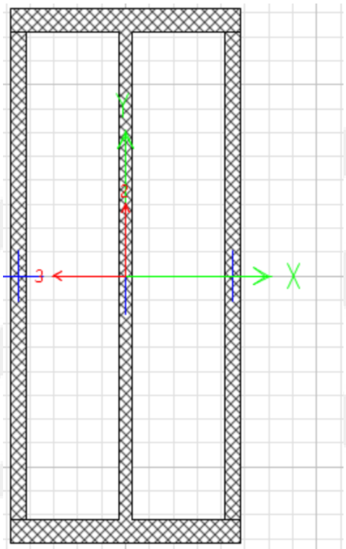

Figure B.2: *HEB700 with Plates*

$$r_x = \sqrt{\frac{I_x}{A}} = \sqrt{\frac{4652 \times 10^6}{93600}} = 223.06 \text{ mm} \tag{B.10}$$

$$r_y = \sqrt{\frac{I_y}{A}} = \sqrt{\frac{1232 \times 10^6}{93600}} = 114.74 \text{ mm} \tag{B.11}$$

$$\lambda_{\text{major}} = \frac{0.85 \times 6.15 \times 1000}{223.06} = 23.45 \tag{B.12}$$

$$\lambda_{\text{minor}} = \frac{0.85 \times 6.15 \times 1000}{114.74} = 45.57 \tag{B.13}$$

$$F_e = \frac{\pi^2 \times 200000}{(45.57)^2} = 950.9 \text{ MPa} \tag{B.14}$$

$$\frac{F_y}{F_e} = \frac{235}{950.9} = 0.247 \tag{B.15}$$

$$F_{cr} = 0.658^{(235/950.9)} \times 235 = 203.00\ \text{MPa} \tag{B.16}$$

$$P_n = F_{cr} \times A_g = 203.00 \times 93600 = 19000.8\ \text{kN} \tag{B.17}$$

$$\phi P_n = 0.90 \times 19000.8 = 17100.7\ \text{kN} \tag{B.18}$$

Slenderness Limits for Beams:

$$\lambda_{\text{flange}} = \frac{b}{2t_f} = \frac{260}{2 \times 17.5} = 7.43 \tag{B.19}$$

$$\lambda_p = 0.38 \times \sqrt{\frac{E}{F_y}} = 11.36 \tag{B.20}$$

$$\lambda_r = 1.0 \times \sqrt{\frac{E}{F_y}} = 29.89 \tag{B.21}$$

$$\lambda_{\text{web}} = \frac{h - 2t_f}{t_w} = \frac{260 - 2 \times 17.5}{10} = 22.5 \tag{B.22}$$

$$\lambda_p = 3.76 \times \sqrt{\frac{E}{F_y}} = 112.40 \tag{B.23}$$

$$\lambda_r = 5.70 \times \sqrt{\frac{E}{F_y}} = 170.39 \tag{B.24}$$

$$\lambda_{\text{flange}} = 7.43 \leq \lambda_p = 11.36 \leq \lambda_r = 29.89 \quad \Rightarrow \quad \text{Compact Section} \tag{B.25}$$

$$\lambda_{\text{web}} = 22.5 \leq \lambda_p = 112.40 \leq \lambda_r = 170.39 \quad \Rightarrow \quad \text{Compact Section} \tag{B.26}$$

Moment Capacity for Beams:

$$M_y = F_y \times S = 235 \times (1148 \times 10^3) = 269.78 \times 10^6\ \text{N·mm} = 269.78\ \text{kN·m} \tag{B.27}$$

$$M_p = F_y \times Z = 235 \times (1283 \times 10^3) = 301.51 \times 10^6\ \text{N·mm} = 301.51\ \text{kN·m} \tag{B.28}$$

$$M_n = M_p \leq 1.5M_y \quad \Rightarrow \quad 301.51 \leq 1.5 \times 269.78 \quad \Rightarrow \quad 301.51 \leq 404.67\ \text{kN·m} \tag{B.29}$$

Shear Capacity for Beams:

$$V_n = 0.60 \times 235\ \text{N/mm}^2 \times (225 \times 10)\ \text{mm}^2 = 317.25\ \text{kN} \tag{B.30}$$

APPENDIX C. MATLAB CODE FOR FAST FOURIER TRANSFORM (FFT)

```
% --- 1. Read Data ---
data = readmatrix("secondcable.xlsx");
t = data(:,1);     % Time vector [s]
y = data(:,2);     % Acceleration vector [g or m/s²]

% --- 2. Sampling Parameters ---
dt = mean(diff(t));     % Time step [s]
Fs = 1 / dt;            % Sampling frequency [Hz]
L = length(y);          % Length of signal
T = L * dt;             % Total duration

% --- 3. Remove DC Offset ---
y = detrend(y);         % Removes linear trend

% --- 4. Bandpass Filter (Butterworth) ---
f_low = 0.5;          % Lower cutoff frequency [Hz]
f_high = 10;          % Upper cutoff frequency [Hz]
order = 4;            % Filter order

% Normalize frequencies for Butterworth filter design
Wn = [f_low f_high] / (Fs/2);
[b, a] = butter(order, Wn, 'bandpass');
y_filtered = filtfilt(b, a, y);  % Zero-phase filtering

% --- 5. FFT on Filtered Signal ---
Y = fft(y_filtered);                 % Compute FFT
P2 = abs(Y / L);                     % Two-sided spectrum
P1 = P2(1:floor(L/2)+1);             % One-sided spectrum
P1(2:end-1) = 2 * P1(2:end-1);       % Correct amplitude
f = Fs * (0:floor(L/2)) / L;         % Frequency vector

% --- 6. Display Sampling Info ---
disp(['Sampling Frequency Fs: ', num2str(Fs), ' Hz']);
disp(['Signal Length: ', num2str(L), ' samples']);
disp(['Signal Duration: ', num2str(T), ' seconds']);

% --- 7. Plot Results ---
figure;
```

```
% Time-domain signal
subplot(2,1,1)
plot(t, y_filtered, 'b')
title('ACC-TIME')
xlabel('Time (s)')
ylabel('Acceleration')
grid on

% Frequency-domain signal (FFT)
subplot(2,1,2)
plot(f, P1)
title('FFT POINT 5 - Z')
xlabel('Frequency (Hz)')
ylabel('|Amplitude|')
xlim([0 10])
grid on
```